

# COMPUTATIONAL EME COMPLIANCE ASSESSMENT OF THE APX SERIES MODEL M37TSS9PW1AN MOBILE RADIO.

**October 26, 2016 (Revised December 15, 2016)** 

Saw Sun Hock, Giorgi Bit-Babik, Ph.D., and Antonio Faraone, Ph.D. Motorola Solutions EME Research Lab, Plantation, Florida

#### Introduction

This report summarizes the computational [numerical modeling] analysis performed to document compliance of the APX Series Model Number M37TSS9PW1AN Mobile Radio and vehicle-mounted antennas with the US Federal Communications Commission (FCC) and Innovation, Science and Economic Development (ISED) Canada guidelines for human exposure to radio frequency (RF) emissions. The radio operates in the following frequency bands:

Regions	Bands	Frequency Band (MHz)
	LMR VHF	150.8 - 173.4
US FCC	LMR UHF1	406.1 - 470
02100	LMR UHF2	450 - 512
	LMR 7/800	769-775; 799-824; 851-869
	LMR VHF	138 - 174
ISED Canada	LMR UHF1	406.1 – 430; 450 -470
ISED Cunada	LMR UHF2	450 -470
	LMR 7/800	769-775; 799-824; 851-869
	LMR VHF	136 - 174
Overall (Other	LMR UHF1	380 - 470
regions)	LMR UHF2	450 -520
	LMR 7/800	764 – 805; 806 -870

This computational analysis supplements the measurements conducted to evaluate the compliance of the exposure from this mobile radio with respect to applicable *maximum* permissible exposure (MPE) limits. All test conditions (51 in total) that did not conform with applicable MPE limits were analyzed to determine whether those conditions complied with the

specific absorption rate (SAR) limits for general public exposure (1.6 W/kg averaged over 1 gram of tissue and 0.08 W/kg averaged over the whole body) set forth in FCC guidelines, which are based on the IEEE C95.1-1999 standard [1]. The same test conditions were also analyzed to determine compliance with the SAR limits set forth in the ICNIRP [3] guidelines and IEEE Std. C95.1-2005 standard [4] (2.0 W/kg averaged over 10 gram of tissue and 0.08 W/kg averaged over the whole body). In total 102 independent simulations had been performed addressing exposure of passenger to the VHF, UHF R1 and UHF R2 mobile radio with trunk/roof-mount antennas.

For all simulations a commercial code based on Finite-Difference-Time-Domain (FDTD) methodology was employed to carry out the computational analysis. It is well established and recognized within the scientific community that SAR is the primary dosimetric quantity used to evaluate the human body's absorption of RF energy and that MPE limits are in fact derived from SAR. Accordingly, the SAR computations provide a scientifically valid and more relevant estimate of human exposure to RF energy.

#### Method

The simulation code employed is XFDTD<sup>TM</sup> v7.3.1, by Remcom Inc., State College, PA. This computational suite provides means to simulate the heterogeneous full human body model defined according to the draft IEC/IEEE 62704-2 standard and derived from the so-called Visible Human [2], discretized in 3 mm voxels. The draft IEC/IEEE 62704-2 standard dielectric properties of 39 body tissues are automatically assigned by XFDTD<sup>TM</sup> at any specific frequency. The "seated" man model was obtained from the standing model by modifying the articulation angles at the hips and the knees. Details of the computational method and model are provided in the Appendix A to this report. The evaluation of the computational uncertainties and results of the benchmark validations are provided in the Appendix B attached to this report. The XFDTD code validation performed according to IEEE/IEC 62704-1 draft standard by Remcom Inc., is provided in conjunction with this report.

The car model has been imported into XFDTD<sup>TM</sup> from the CAD file of a sedan car having dimensions 4.98 m (L) x 1.85 m (W) x 1.18 m (H), and discretized with the minimum resolution of 3 mm and the maximum resolution of 9 mm. The Figure 1 below show both the

CAD model and the photo of the actual car This CAD model has been incorporated into the IEC/IEEE 62704-2 draft standard.

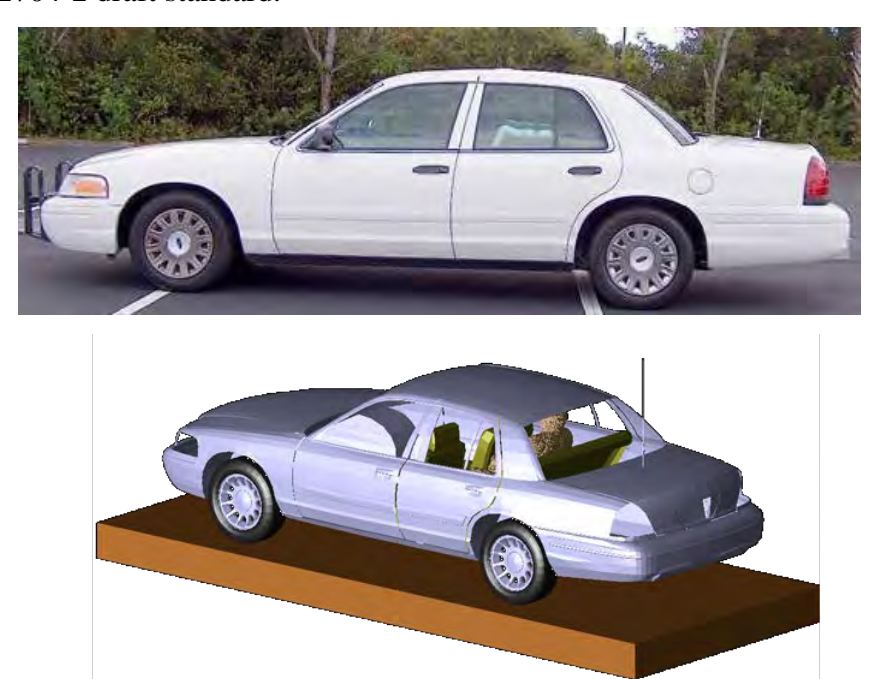


Figure 1: The photo picture of the car used in field measurements and the corresponding CAD model used in simulations

For bystander exposure, the antenna position is in the center of the trunk, so as to replicate the experimental conditions used in MPE measurements. Figure 2 shows some of the the XFDTD<sup>TM</sup> computational models used for bystander exposure.

For passenger exposure, the antenna position is on the trunk and the distance of trunk mounted antenna from the passenger head when the passenger is located in the center of the back seat was set at 85 cm, to replicate the experimental conditions used in MPE measurements. Figure 3 shows some of the XFDTD<sup>TM</sup> computational models used for passenger exposure to trunk mounted antennas

According to the IEC/IEEE 62704-2 draft standard (December 11, 2015) for exposure simulations from vehicle mount antennas the lossy dielectric slab with 30 cm thickness,

dielectric constant of 8 and conductivity of 0.01 S/m has been introduced in the computational model to properly account for the effect of the ground (pavement) on exposure.

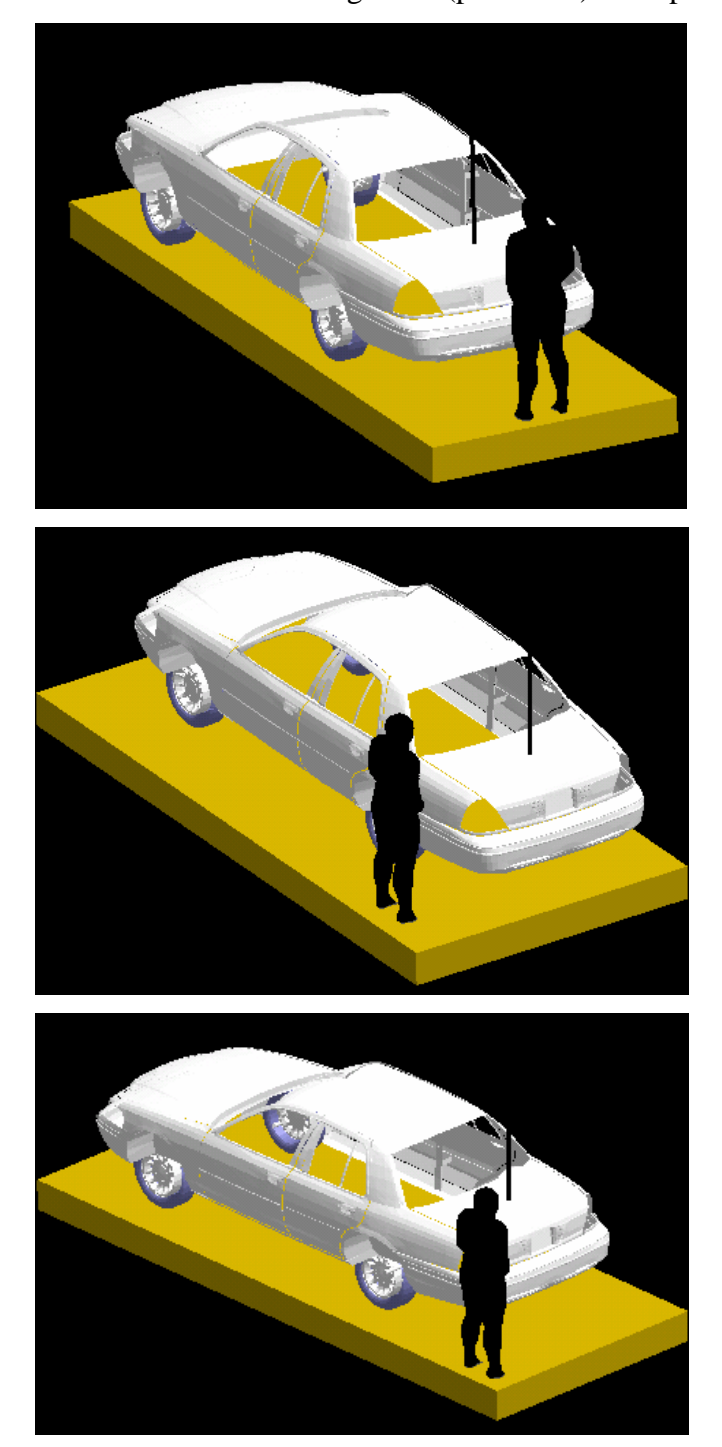


Figure 2: Bystander model exposed to a trunk-mount antenna: Bystander is located at the back, on the side or at the corner of the car replicating the measurement conditions. The antenna is mounted in the center of the trunk. The dielectric slab under the car is introduced to model the ground (pavement) effect on exposure.

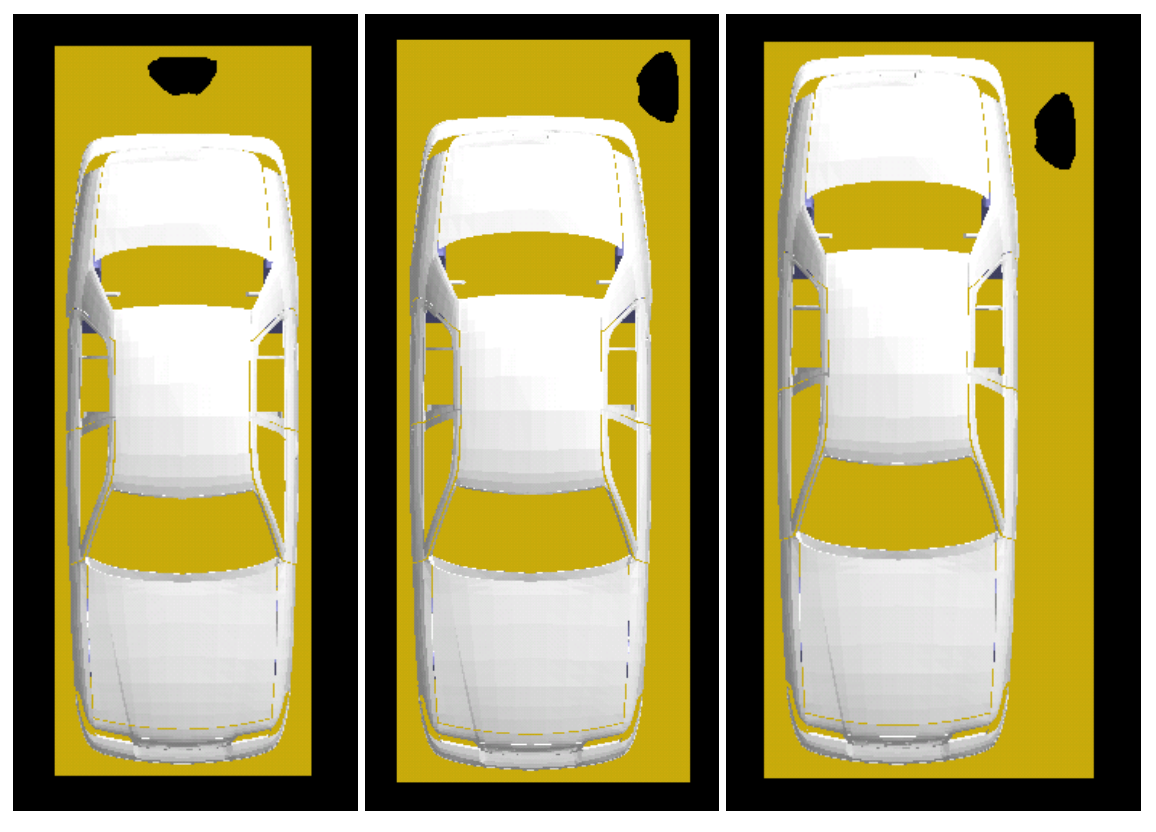
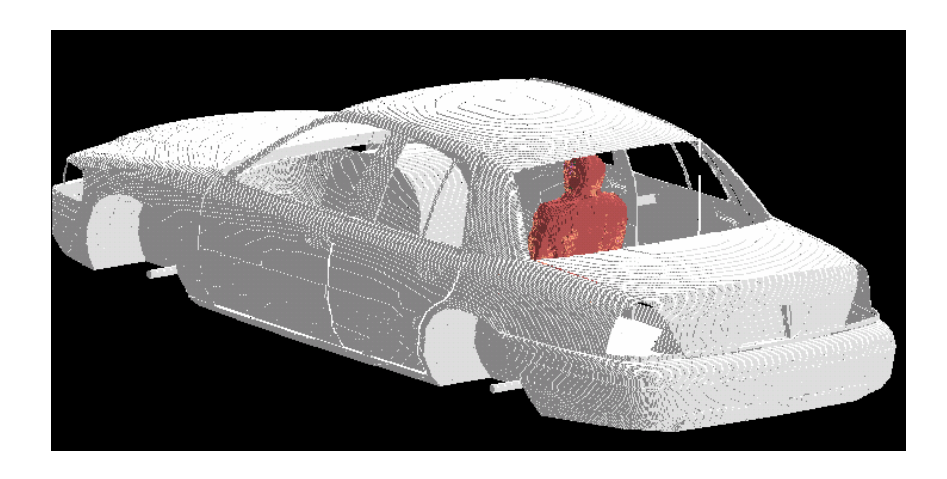


Figure 3: Top view of bystander exposure model four different locations relative to the vehicle model that replicate the measurement conditions.



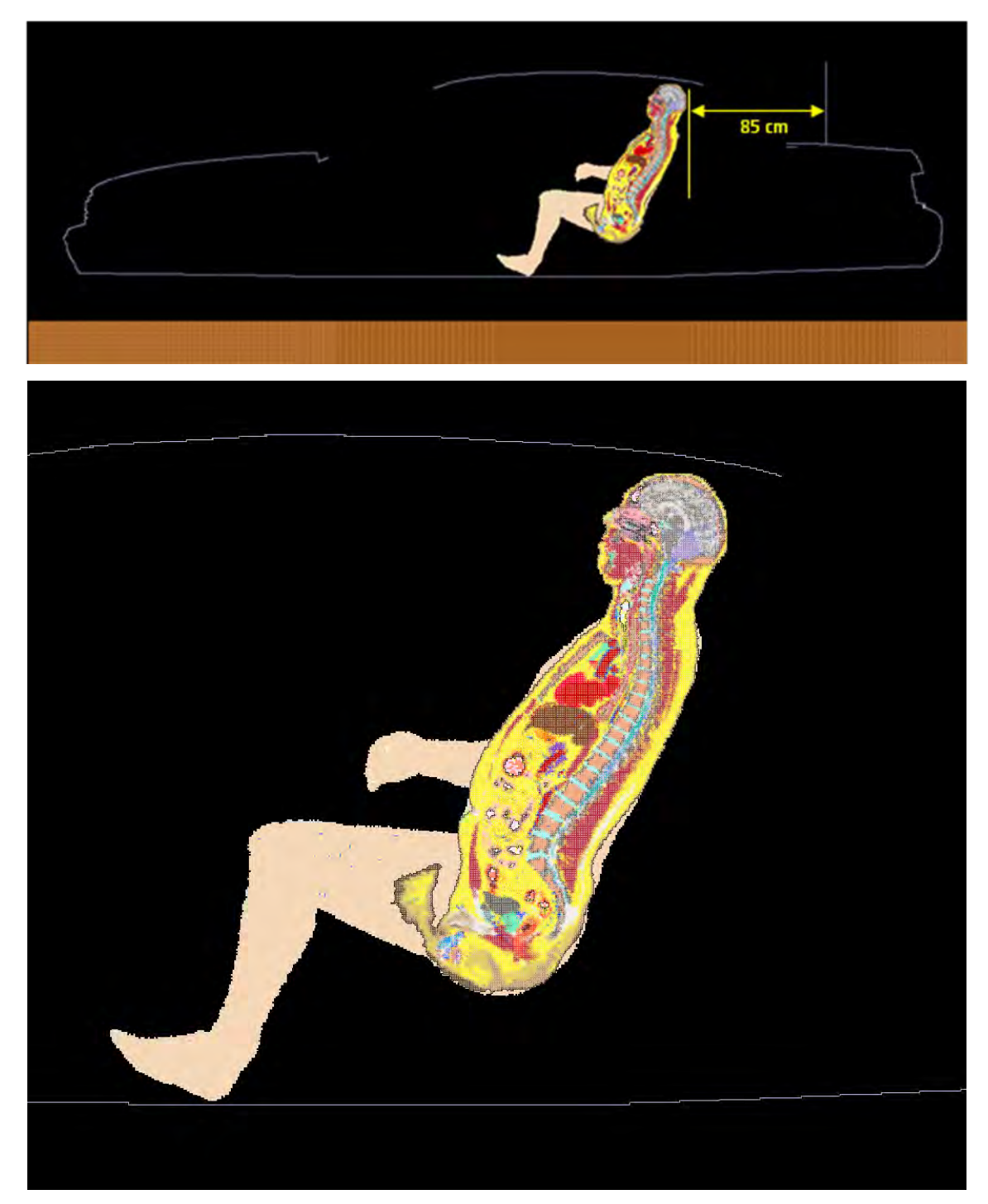


Figure 4: Passenger model exposed to a trunk-mount antenna: XFDTD geometry.

The antenna is mounted at 85 cm from the passenger located in the center of the back seat.

The computational code employs a time-harmonic excitation to produce a steady state electromagnetic field in the exposed body. Subsequently, the corresponding SAR distribution is automatically processed in order to determine the whole-body, 1-g, and 10-g average SAR. The

maximum average output power from mobile radio antenna is 60W (136-174MHz), 54W (380-484MHz), 48W (485-512MHz) and 30W (512-520MHz). Since the ohmic losses in the car materials, as well as the mismatch losses at the antenna feed-point are neglected, and sourcebased time averaging (50% talk time) is employed, all computational results are normalized to half of it, i.e., 30W (136-174MHz), 27W (380-484MHz), 24W (485-512MHz) and 15W (512-520MHz) average net output power; less the corresponding minimum insertion loss in excess of 0.5 dB of the feed cables supplied with the antennas. This power normalization is in accordance with the IEC/IEEE 62704-2 draft standard (August, 2016).

#### Results of SAR computations for car passengers and bystanders

The test conditions requiring SAR computations are summarized in Table 1, together with the antenna data, the SAR results, and power density (P.D.) as obtained from the measurements in the corresponding test conditions. The conditions are for antennas mounted on the trunk. The antenna length in Table 1 includes the 1.8 cm magnetic mount base used in measurements to position the antenna on the vehicle. The same length was used in simulation model.

The passenger is located in the center or on the side of the rear seat. The passenger model is surrounded by air, as the seat, which is made out of poorly conductive fabrics, is not included in the computational model.

The bystander is located at the measurement distance from the transmit antenna as described in the original report and is assessed separately for front and back (rear) exposure.

All the transmit frequency, antenna length, and passenger location combinations reported in Table 1 have been simulated individually. This table also includes the interpolated adjustment factor and corresponding SAR scaled values following requirement of the draft IEC/IEEE 62704-2 draft standard.

Table 1: Results of the Computations and Adjusted SAR for passenger/bystander exposure (50% talk-time)

Mount	Antenna Kit#	Antenna Length	Freq	P.D.	Exposure Location	Com	putations (W/kg)	SAR		terpolate tment Fa		Adjusted	SAR Resu	lts (W/kg)					
Location	1	(cm)	(MHz)	(mW/cm^2)	Emposure Escuron	1 g	10 g	WB	1 g	10 g	WB	1 g	10 g	WB					
				0.14	Bystander 0 deg Front	0.22	0.14	0.007	1.32	1.32	1.924	0.29	0.18	0.013					
		110.2	150.0125	0.14	Bystander 0 deg Rear	0.38	0.19	0.007	1.32	1.32	1.924	0.50	0.25	0.013					
		118.3	158.0125	0.15	Back Center	0.11	0.07	0.005	1.91	2.01	2.411	0.21	0.14	0.012					
					Back Side	0.09	0.05	0.004	4.14	4.34	2.989	0.37	0.22	0.012					
		114.3	165.0125	0.16	Back Center	0.15	0.10	0.005	1.93	2.02	2.420	0.29	0.20	0.012					
		114.3	165.0125	0.16	Back Side	0.08	0.05	0.003	4.09	4.29	2.980	0.33	0.21	0.009					
Trunk	RAD4010ARB,			0.15	Bystander 0 deg Front	0.17	0.11	0.008	1.35	1.35	1.969	0.23	0.15	0.016					
	1/2 Wave (136- 174MHz)				Bystander 0 deg Rear	0.37	0.19	0.007	1.35	1.35	1.969	0.50	0.26	0.014					
				0.16	Bystander 45 deg Front	0.22	0.12	0.007	1.35	1.35	1.969	0.30	0.16	0.014					
		105.5	172 0125		Bystander 45 deg Rear	0.30	0.17	0.007	1.35	1.35	1.969	0.40	0.23	0.014					
		105.5	173.0125	0.16	Bystander 90 deg Front	0.32	0.21	0.013	1.35	1.35	1.969	0.43	0.28	0.026					
				0.16	Bystander 90 deg Rear	0.63	0.33	0.013	1.35	1.35	1.969	0.85	0.44	0.026					
					Back Center	0.20	0.12	0.008	1.94	2.03	2.431	0.39	0.24	0.019					
				0.20	Back Side	0.15	0.08	0.006	4.03	4.24	2.969	0.60	0.34	0.018					
		120.3	120.2	120.2				(1)		Back Center	0.43	0.27	0.018	1.82	1.91	2.314	0.78	0.52	0.042
			<sup>(1)</sup> 144.0000	0.21	Back Side	0.15	0.10	0.011	3.93	4.11	2.829	0.59	0.41	0.031					
		115.8		0.21	Back Center	0.28	0.17	0.012	1.90	2.00	2.401	0.53	0.34	0.029					
			150.8000		Back Side	0.14	0.08	0.008	4.19	4.39	2.999	0.59	0.35	0.024					
		104.5		0.13	Bystander 0 deg Front	0.22	0.14	0.008	1.32	1.32	1.924	0.29	0.18	0.015					
Trunk	HAD4022A, 5/8		104.5 158.0125		Bystander 0 deg Rear	0.36	0.18	0.008	1.32	1.32	1.924	0.47	0.24	0.015					
Trunk	Wave (132- 174MHz)				Back Center	0.33	0.20	0.014	1.91	2.01	2.411	0.63	0.40	0.034					
					Back Side	0.22	0.15	0.012	4.14	4.34	2.989	0.91	0.65	0.036					
					Back Center	0.40	0.25	0.017	1.93	2.02	2.420	0.77	0.51	0.041					
		98.3	165.0125	0.50	Back Side	0.26	0.23	0.012	4.09	4.29	2.980	1.06	0.99	0.036					
					Back Center	0.37	0.23	0.017	1.94	2.03	2.431	0.72	0.47	0.041					
		91.7	173.0125	0.44	Back Side	0.31	0.19	0.013	4.03	4.24	2.969	1.25	0.81	0.039					
					Bystander 0 deg Front	0.15	0.10	0.006	1.27	1.28	4.329	0.19	0.13	0.026					
			<sup>(1)</sup> 144.0000	0.18	Bystander 0 deg Rear	0.19	0.09	0.006	1.27	1.28	4.329	0.24	0.12	0.026					
	HAD4016A, 1/4				Bystander 0 deg Front	0.21	0.14	0.010	1.30	1.30	4.493	0.27	0.18	0.045					
Roof	Wave (136- 162MHz)	53.1	150.8000	0.17	Bystander 0 deg Rear	0.22	0.11	0.009	1.30	1.30	4.493	0.29	0.14	0.040					
	162MHZ)				Bystander 0 deg Front	0.18	0.12	0.009	1.30	1.31	4.447	0.23	0.16	0.040					
			156.4000	0.16	Bystander 0 deg Rear	0.20	0.10	0.009	1.30	1.31	4.447	0.26	0.13	0.040					
					Bystander 0 deg Front	0.15	0.10	0.006	1.27	1.28	4.329	0.19	0.13	0.026					
n	HAD4021A, 1/4			0.17	Bystander 0 deg Rear	0.13	0.10	0.006	1.27	1.28	4.329	0.19	0.13	0.026					
Roof	Wave (136- 174MHz)	53.5	<sup>(1)</sup> 144.0000		Back Center	0.19	0.09	0.006	1.18	1.00	1.914	0.24	0.12	0.020					
	1 /41/1112)			0.14	Back Side	0.18	0.16	0.006	1.18	1.00	1.491	0.21	0.16	0.011					
	<u> </u>			Dack Side	0.20	0.22	0.003	1.00	1.00	1.471	0.20	0.22	0.007						

**Table 1 (Continued)** 

		Antenna			Table 1 (Conti		) putations	CAD	In	terpolate	d							
Mount	Antenna Kit#	Length	Freq (MHz)	P.D. (mW/cm^2)	Exposure Location	Com	(W/kg)	SAK		tment Fa		Adjusted	SAR Resu	lts (W/kg)				
Location		(cm)		(III vv/cIII · · 2)		1 g	10 g	WB	1 g	10 g	WB	1 g	10 g	WB				
			150.8000	0.16	Bystander 0 deg Front	0.21	0.14	0.007	1.30	1.30	4.493	0.27	0.18	0.031				
Roof	HAD4021A, 1/4 Wave (136-	53.5		0.00	Bystander 0 deg Rear	0.22	0.11	0.009	1.30	1.30	4.493	0.29	0.14	0.040				
	174MHz)	23.0	158.0125	0.14	Back Center	0.09	0.08	0.002	1.27	1.07	2.072	0.11	0.09	0.004				
			136.0123	0.14	Back Side	0.15	0.13	0.002	1.02	1.03	1.532	0.15	0.13	0.003				
					Bystander 0 deg Front	0.16	0.10	0.005	1.28	1.29	4.386	0.21	0.13	0.022				
			(1)146.0000	0.17	Bystander 0 deg Rear	0.19	0.10	0.006	1.28	1.29	4.386	0.24	0.13	0.026				
Roof	AN000131A01,				Bystander 0 deg Front	0.21	0.14	0.008	1.30	1.30	4.493	0.27	0.18	0.036				
	1/4 Wave (136- 870MHz)	57.5	150.8000	0.16	Bystander 0 deg Rear	0.23	0.12	0.008	1.30	1.30	4.493	0.30	0.16	0.036				
					Bystander 0 deg Front	0.19	0.13	0.008	1.31	1.31	4.433	0.25	0.17	0.035				
			158.0125	0.15	Bystander 0 deg Rear	0.23	0.13	0.009	1.31	1.31	4.433	0.30	0.17	0.040				
					Bystander 0 deg Kear	0.23	0.12	0.009	1.31	1.31	4.433	0.30	0.10	0.040				
			158.0125	0.15	Bystander 0 deg Front	0.17	0.12	0.008	1.31	1.31	4.433	0.22	0.16	0.035				
	**************				Bystander 0 deg Rear	0.20	0.10	0.009	1.31	1.31	4.433	0.26	0.13	0.040				
Roof	HAD4017A, 1/4 Wave (146-	48	165.0125	0.14	Bystander 0 deg Front	0.17	0.11	0.010	1.31	1.33	4.375	0.22	0.15	0.044				
	174MHz)				Bystander 0 deg Rear	0.30	0.15	0.010	1.31	1.33	4.375	0.39	0.20	0.044				
			173.0125	0.15	Bystander 0 deg Front	0.27	0.16	0.014	1.32	1.34	4.308	0.36	0.21	0.060				
					Bystander 0 deg Rear	0.44	0.23	0.014	1.32	1.34	4.308	0.58	0.31	0.060				
		30.8					406.5000	0.28	Back Center	0.55	0.37	0.015	2.33	2.34	2.742	1.28	0.87	0.041
			400.3000	0.28	Back Side	0.60	0.41	0.013	2.32	2.60	2.658	1.39	1.07	0.035				
			422.0125	0.24	Back Center	0.19	0.13	0.011	2.35	2.36	2.763	0.45	0.31	0.030				
					Back Side	0.30	0.20	0.013	2.21	2.50	2.637	0.66	0.50	0.034				
			(2)438.0125	0.28	Back Center	0.29	0.20	0.014	2.38	2.38	2.784	0.69	0.48	0.039				
Trunk	HAE6013A, 1/2 Wave (380-			0.28	Back Side	0.40	0.26	0.012	2.09	2.38	2.616	0.84	0.62	0.031				
	470MHz)		450.0125	0.37	Back Center	0.40	0.28	0.018	2.40	2.40	2.800	0.96	0.67	0.050				
			430.0123	0.37	Back Side	0.29	0.19	0.014	2.00	2.30	2.600	0.58	0.44	0.036				
			460.0000	0.34	Back Center	0.16	0.12	0.013	2.36	2.36	2.783	0.38	0.28	0.036				
				460.0000	0.54	Back Side	0.32	0.22	0.015	1.98	2.27	2.580	0.63	0.50	0.039			
				469.9875	0.37	Back Center	0.37	0.24	0.012	2.32	2.32	2.766	0.86	0.56	0.033			
							103.5075	0.07	Back Side	0.19	0.16	0.012	1.97	2.24	2.560	0.37	0.36	0.031
			(1)(2) 380.0125	0.21	Back Center	0.16	0.12	0.010	2.28	2.31	2.707	0.37	0.28	0.027				
			380.0125	0.21	Back Side	0.28	0.15	0.010	2.51	2.79	2.693	0.70	0.42	0.027				
				0.16	Bystander 0 deg Front	0.30	0.24	0.011	1.53	1.74	1.640	0.46	0.42	0.018				
				0.16	Bystander 0 deg Rear	0.14	0.09	0.012	1.53	1.74	1.640	0.21	0.16	0.020				
					Bystander 45 deg Front	0.21	0.15	0.008	1.53	1.74	1.640	0.32	0.26	0.013				
			406.5000	0.20	Bystander 45 deg Rear	0.22	0.18	0.008	1.53	1.74	1.640	0.34	0.31	0.013				
					Back Center	0.55	0.37	0.015	2.33	2.34	2.742	1.28	0.87	0.041				
	HAE6031A, 1/2			0.30	Back Side	0.60	0.41	0.013	2.32	2.60	2.658	1.38	1.07	0.035				
Trunk	Wave (380-	29.8			Back Center	0.19	0.13	0.011	2.35	2.36	2.763	0.45	0.31	0.030				
	520MHz)		422.0125	0.23	Back Side	0.30	0.20	0.013	2.21	2.50	2.637	0.66	0.50	0.034				
					Back Center	0.40	0.28	0.018	2.40	2.40	2.800	0.95	0.67	0.050				
			450.0125	0.42	Back Side	0.29	0.19	0.014	2.00	2.30	2.600	0.58	0.44	0.036				
					Back Center	0.29	0.19	0.014	2.32	2.32	2.766	0.38	0.56	0.033				
			469.9875	0.43														
					Back Side	0.19	0.16	0.012	1.97	2.24	2.560	0.37	0.36	0.031				
			<sup>(2)</sup> 482.5000	0.29	Back Center	0.19	0.14	0.012	2.27	2.27	2.744	0.43	0.32	0.033				
			(2) 482.5000	0.29	Back Side	0.26	0.18	0.015	1.94	2.20	2.535	0.51	0.40	0.038				

Report ID: P3466-EME-00009

# **Table 1 (Continued)**

Mount	Antenna Kit#	Antenna Length	Freq (MHz)	P.D. (mW/cm^2)	Exposure Location	Computations SAR (W/kg)		Interpolated Adjustment Factors			Adjusted SAR Results (W/kg)					
Location		(cm)		(mw/cm^2)		1 g	10 g	WB	1 g	10 g	WB	1 g	10 g	WB		
			406.5000	0.17	Back Center	0.21	0.14	0.011	2.33	2.34	2.742	0.49	0.33	0.030		
			400.3000	0.17	Back Side	0.28	0.16	0.010	2.32	2.60	2.658	0.65	0.42	0.027		
Trunk	AN000131A01, 1/4 Wave (136-	57.5	450.0125	0.28	Back Center	0.32	0.19	0.017	2.40	2.40	2.800	0.77	0.46	0.048		
	870MHz)	37.3	430.0123	0.28	Back Side	0.25	0.15	0.013	2.00	2.30	2.600	0.50	0.34	0.034		
			460.0075	0.20	Back Center	0.10	0.07	0.009	2.32	2.32	2.766	0.23	0.16	0.025		
			469.9875	0.30	Back Side	0.15	0.12	0.009	1.97	2.24	2.560	0.29	0.27	0.023		
			406.5000	0.19	Back Center	0.24	0.17	0.013	2.33	2.34	2.742	0.56	0.40	0.036		
Trunk	HAE6010A, 1/2 Wave (380-	65.3	400.3000	0.19	Back Side	0.28	0.15	0.011	2.32	2.60	2.658	0.65	0.39	0.029		
	433MHz)	65.3	65.3	65.3	419.5000	0.19	Back Center	0.12	0.08	0.009	2.35	2.36	2.759	0.28	0.19	0.025
							419.3000	0.19	Back Side	0.25	0.15	0.012	2.22	2.51	2.641	0.56
Trunk	HAE4011A, 1/2 Wave (450-	75	450.0125	0.20	Back Center	0.23	0.16	0.008	2.40	2.40	2.800	0.55	0.39	0.022		
	470MHz)		73	450.0125	0.20	Back Side	0.26	0.18	0.007	2.00	2.30	2.600	0.51	0.41	0.018	
				450.0125	0.25	Back Center	0.39	0.28	0.018	2.40	2.40	2.800	0.94	0.67	0.050	
				450.0125	450.0125 0.35	Back Side	0.29	0.19	0.014	2.00	2.30	2.600	0.58	0.44	0.036	
			460.0000	0.34	Back Center	0.16	0.12	0.013	2.36	2.36	2.783	0.38	0.28	0.036		
Trunk	HAE6015A, 1/2 Wave (450-	28	400.0000	0.34	Back Side	0.32	0.22	0.015	1.98	2.27	2.580	0.63	0.50	0.039		
	520MHz)	20	469.9875	0.35	Back Center	0.34	0.23	0.012	2.32	2.32	2.766	0.79	0.53	0.033		
			409.9073	0.33	Back Side	0.19	0.15	0.012	1.97	2.24	2.560	0.37	0.34	0.031		
			<sup>(2)</sup> 482.5000	0.28	Back Center	0.18	0.13	0.011	2.27	2.27	2.744	0.41	0.30	0.030		
			402.5000	0.20	Back Side	0.25	0.17	0.015	1.94	2.20	2.535	0.49	0.37	0.038		
Trunk	HAE4012A, 1/2				Back Center	0.45	0.31	0.008	2.32	2.32	2.766	1.04	0.71	0.022		
HUHK	Wave (470- 495MHz)	70.3	470.0125	0.26	Back Side	0.15	0.10	0.008	1.97	2.24	2.560	0.29	0.23	0.020		

Notes:

Frequency not regulated by FCC.
 Frequency not regulated by ISED Canada.
 Bold Blue – the highest SAR results computed for the respective frequency bands

The SAR distribution in the exposure condition that gave highest adjusted 1-g SAR for VHF Band is reported in Figure 5 (173.0125 MHz, passenger on the side of the back seat, HAD4022A antenna).

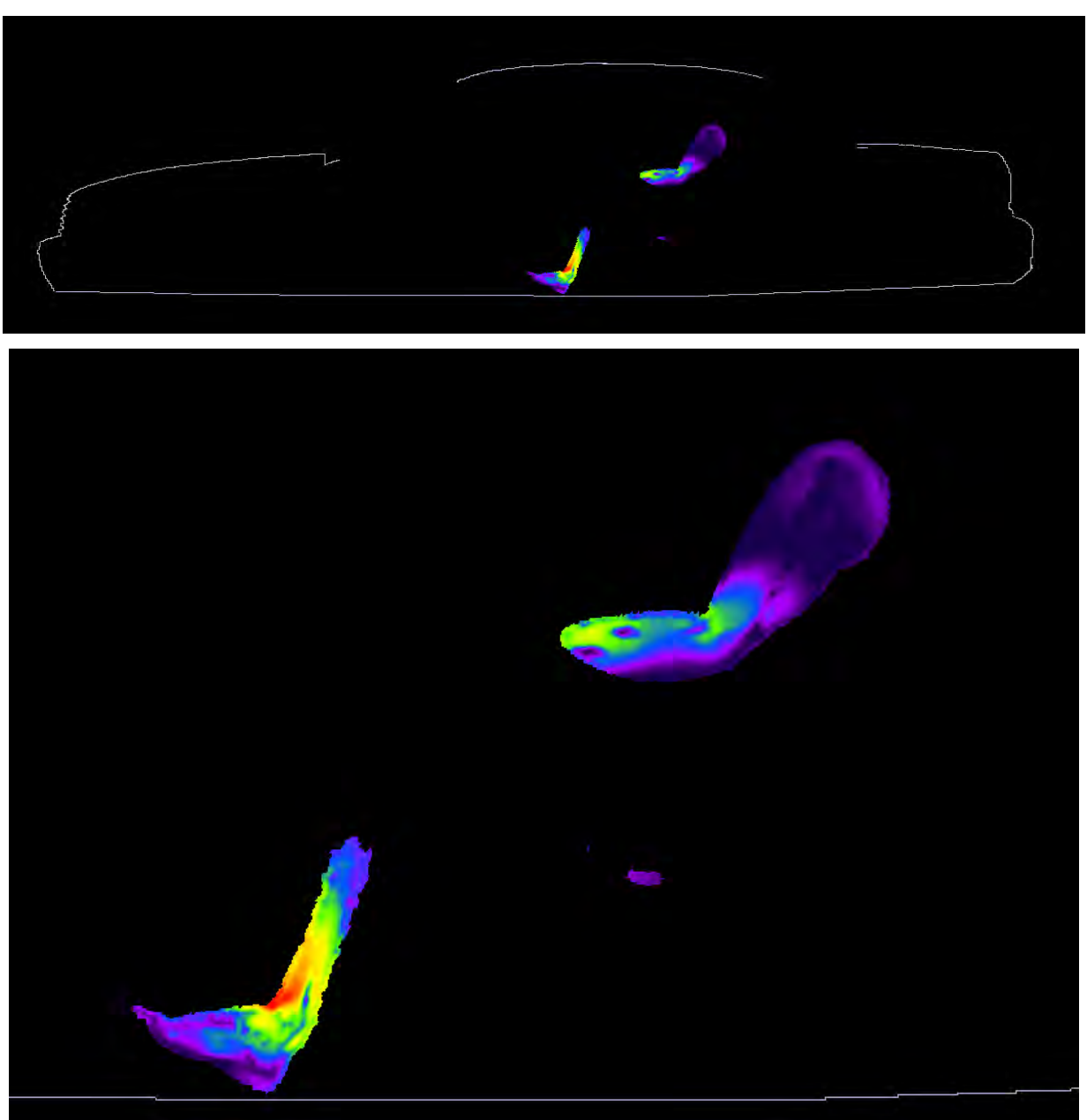
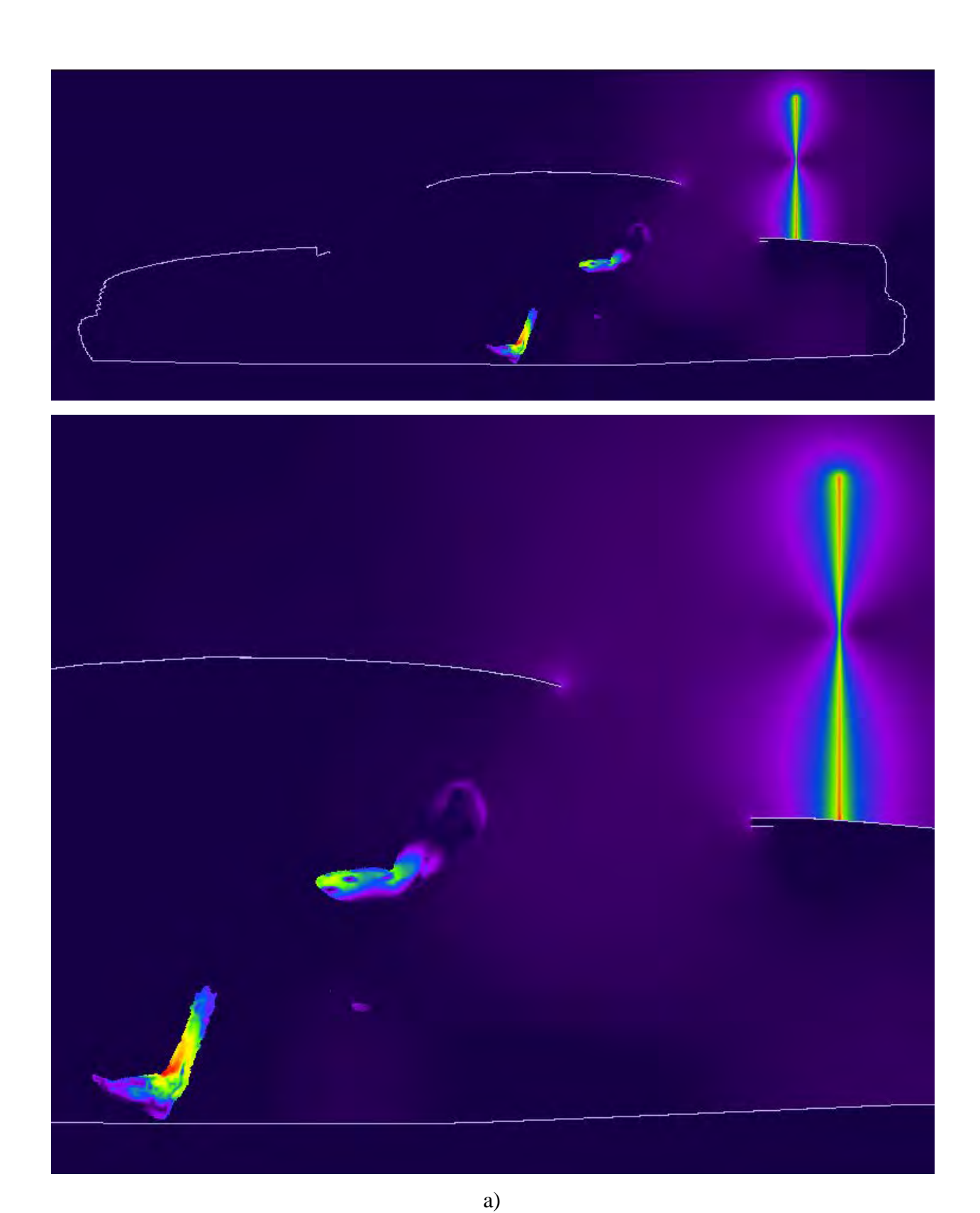


Figure 5. SAR distribution at 173.0125 MHz in the passenger model located on the side of the back seat, produced by the trunk-mount HAD4022A antenna. The contour plot is relative to the plane where the peak 1-g average SAR for this exposure condition occurs.

The two pictures below in Figure 6 show the E and H field distributions in the plane of the antenna corresponding to the condition in Figure 5.



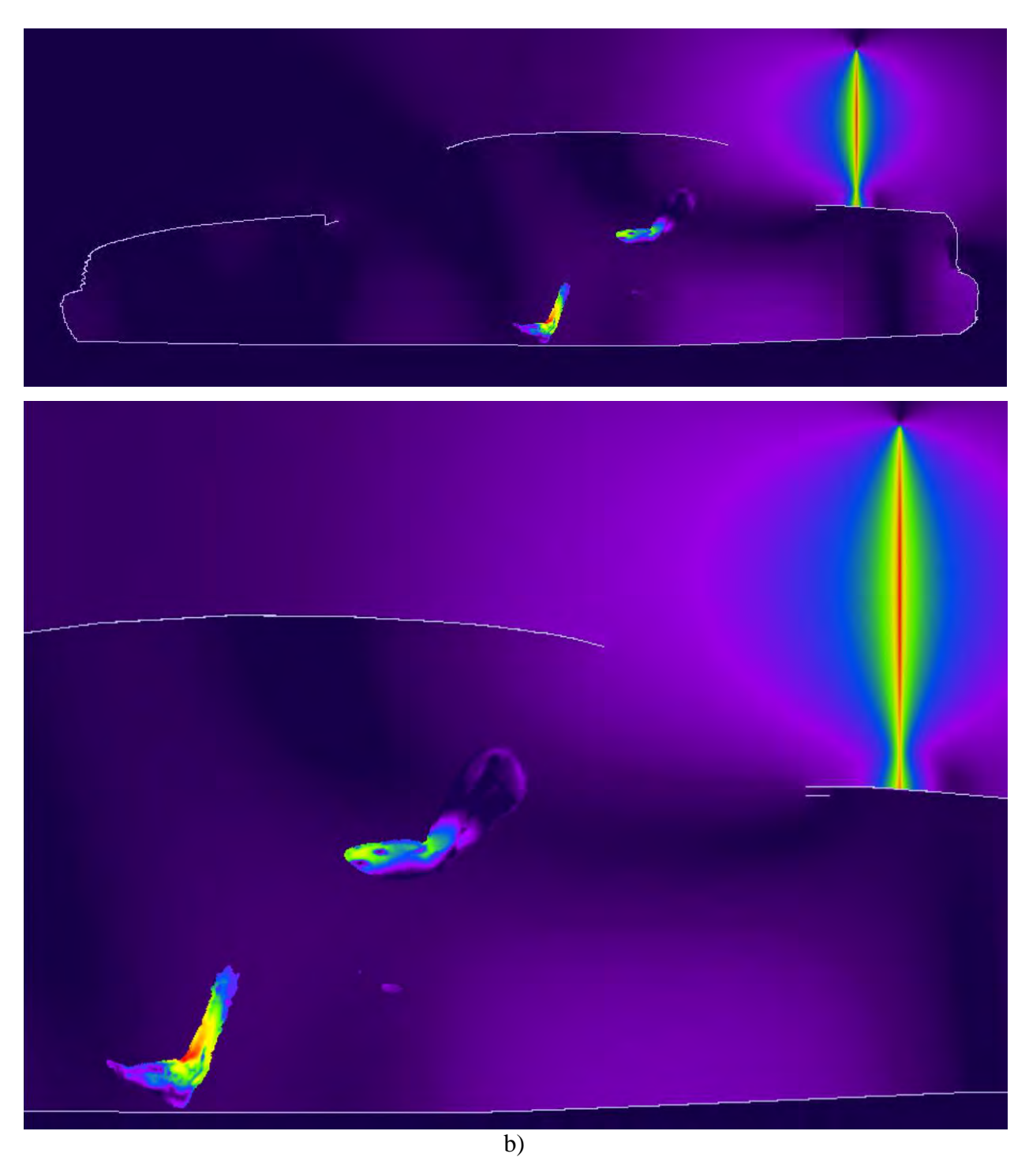


Figure 6. (a) E-field magnitude distribution corresponding to exposure condition of Figure 5, and (b) H-field magnitude distribution corresponding to exposure condition of Figure 5.

The highest adjusted 1-g SAR was produced in the passenger exposure condition with HAD4022A antenna at 173.0125 MHz (passenger on the side of the back seat).

The SAR distribution in the exposure condition that gave highest adjusted 1-g SAR for UHF R1 Band is reported in Figure 7 (406.5 MHz, passenger on the side of the back seat, HAE6013A antenna).

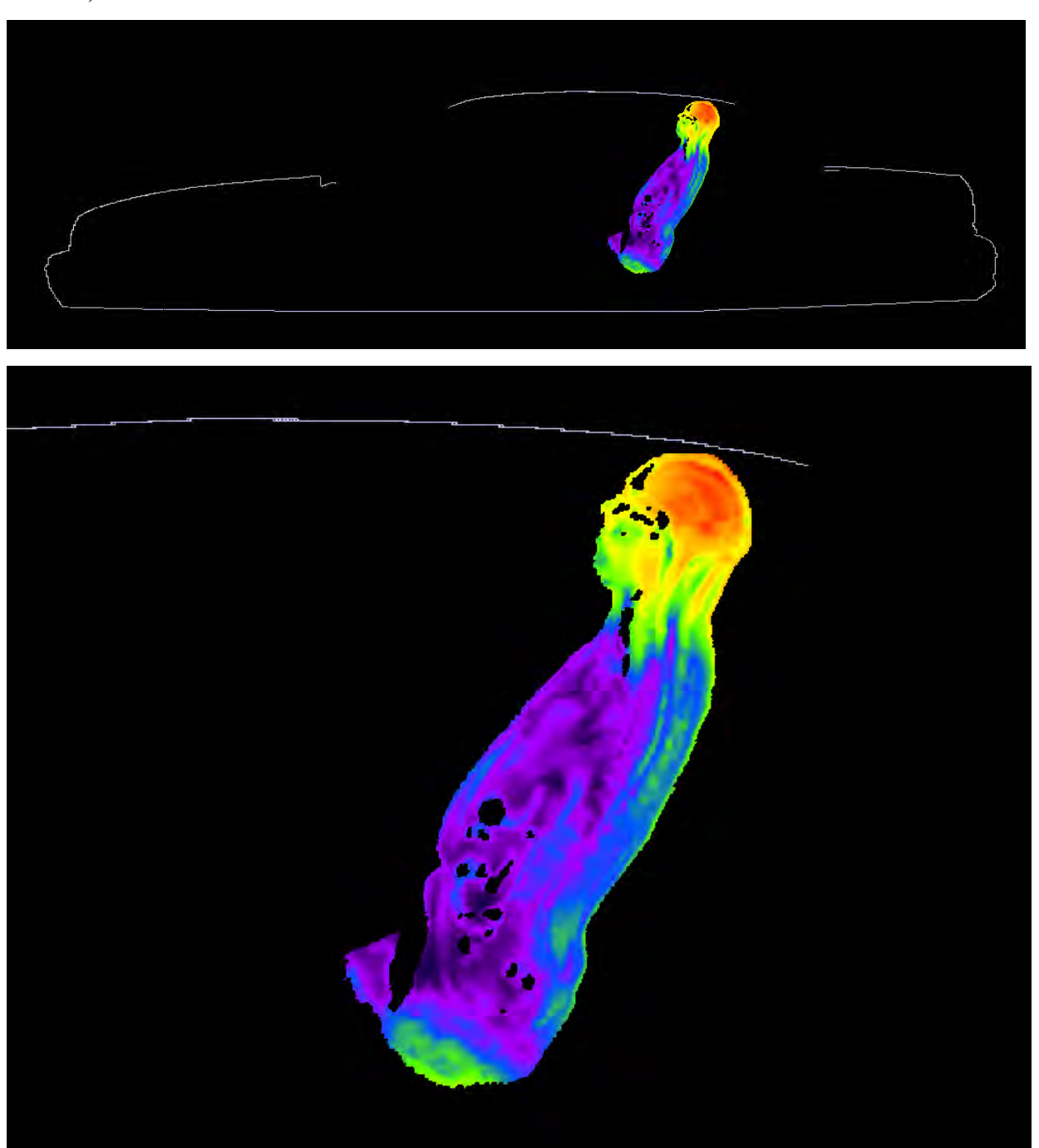
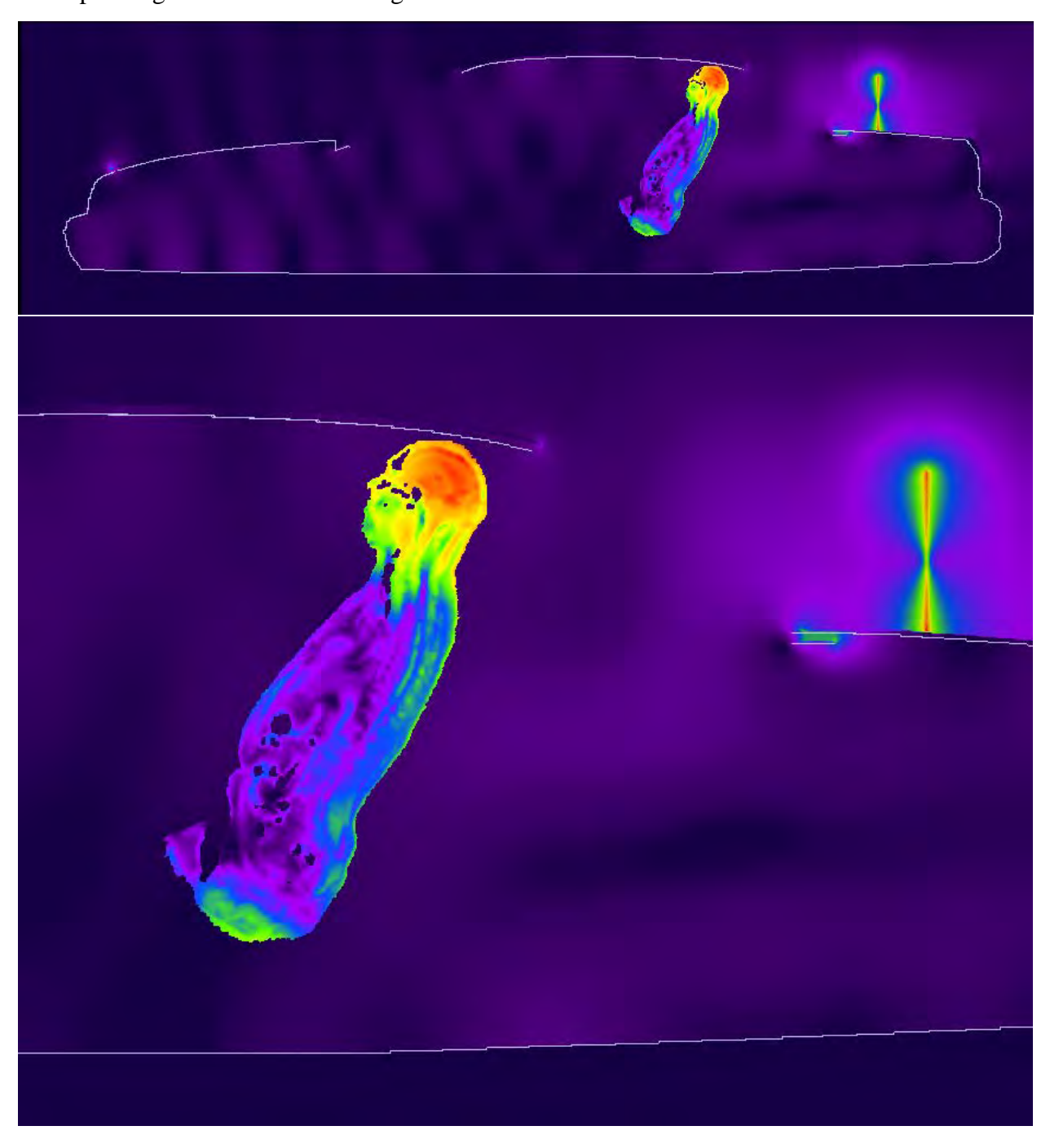


Figure 7. SAR distribution at 406.5 MHz in the passenger model located on the side of the back seat, produced by the trunk-mount HAE6013A antenna. The contour plot is relative to the plane where the peak 1-g average SAR for this exposure condition occurs.

The pictures below in Figure 8 show the E and H field distributions in the plane of the antenna corresponding to the condition in Figure 7



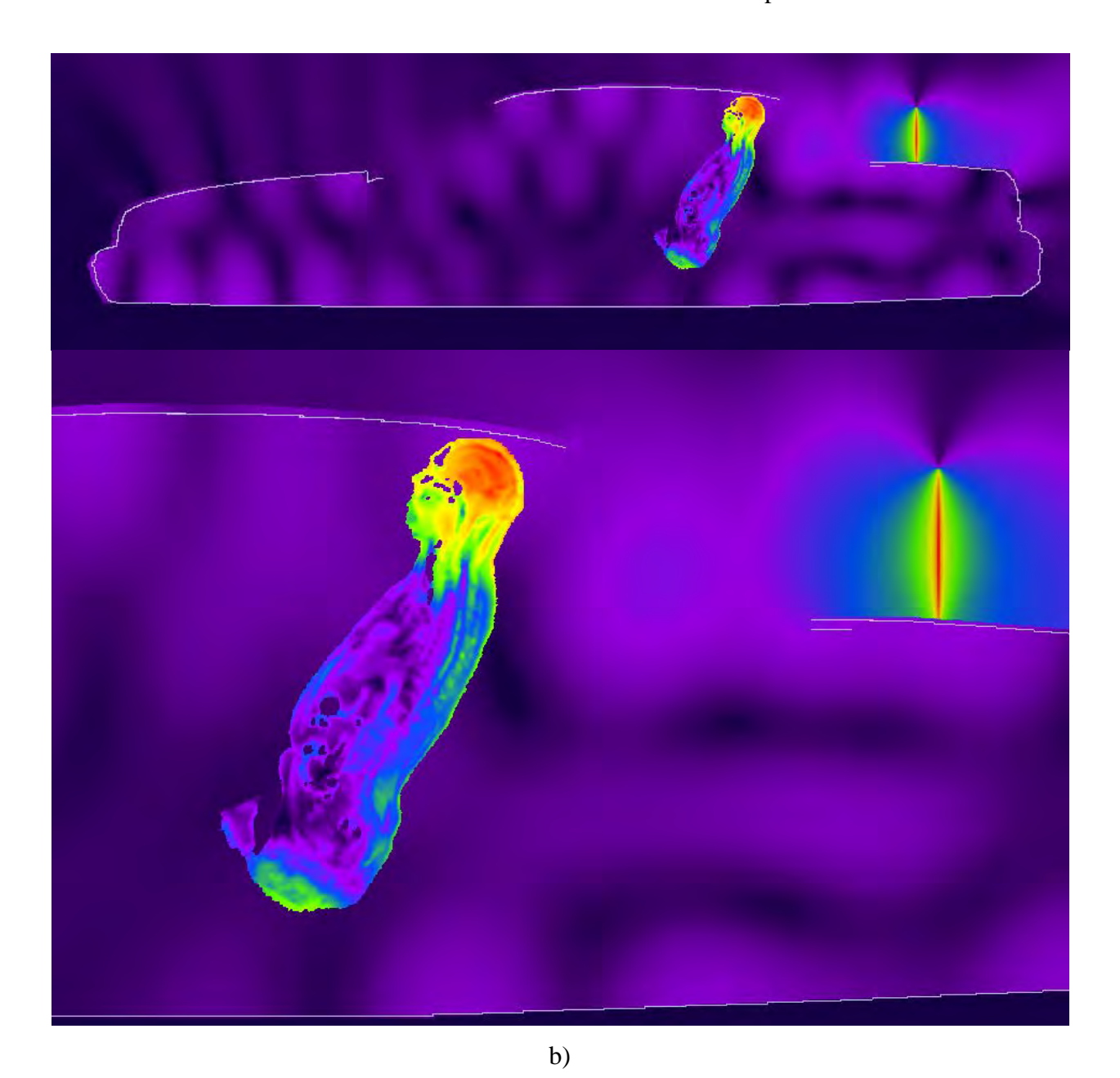


Figure 8. (a) E-field magnitude distribution corresponding to exposure condition of Figure 7, and (b) H-field magnitude distribution corresponding to exposure condition of Figure 7.

The highest adjusted 1-g SAR was produced in the passenger exposure condition with HAE6013A antenna at 406.5 MHz (passenger on the side of the back seat).

The SAR distribution in the exposure condition that gave highest adjusted 1-g SAR for UHF R2 Band is reported in Figure 9 (450.0125 MHz, passenger on the center of the back seat, HAE6013A antenna).

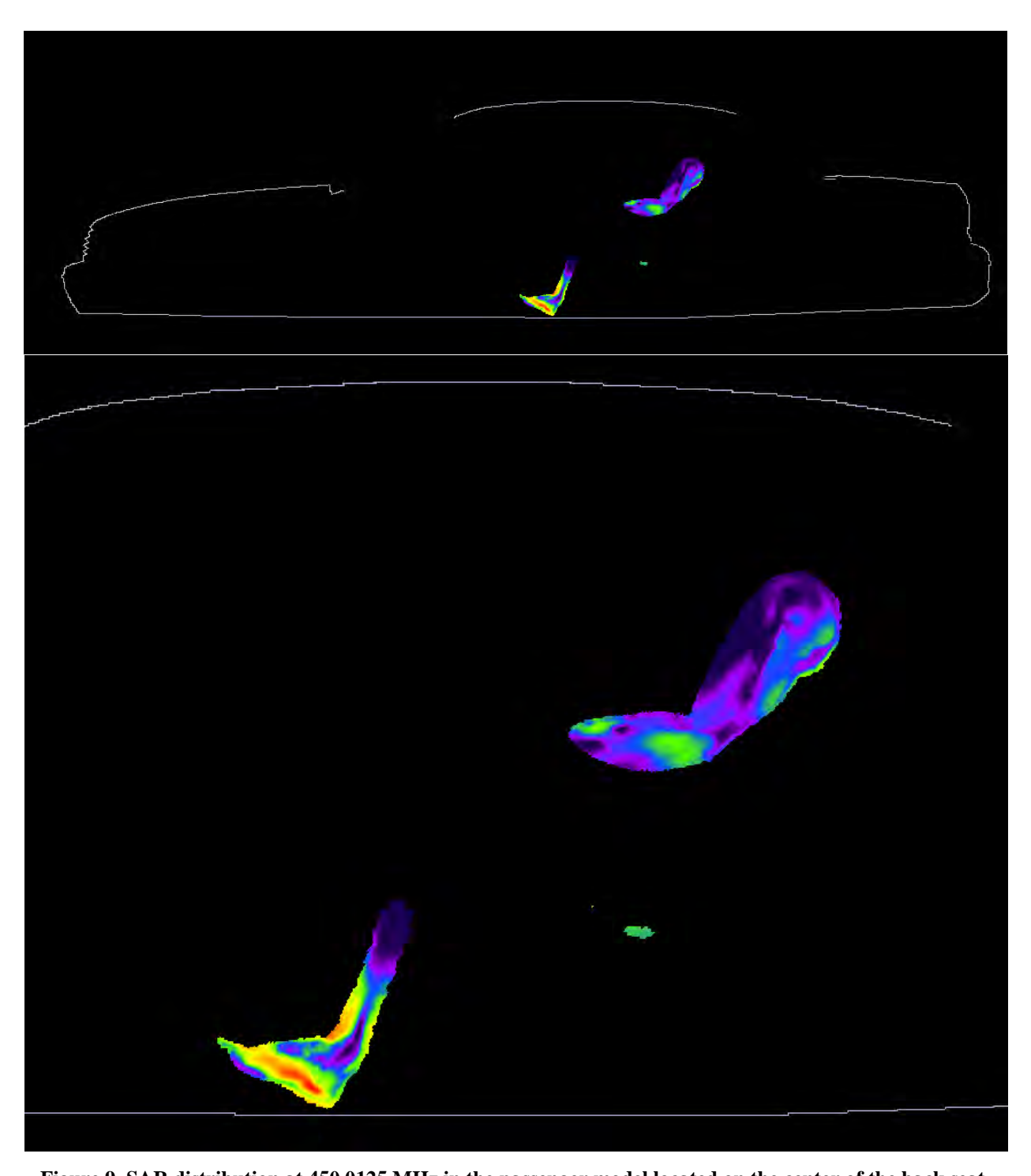
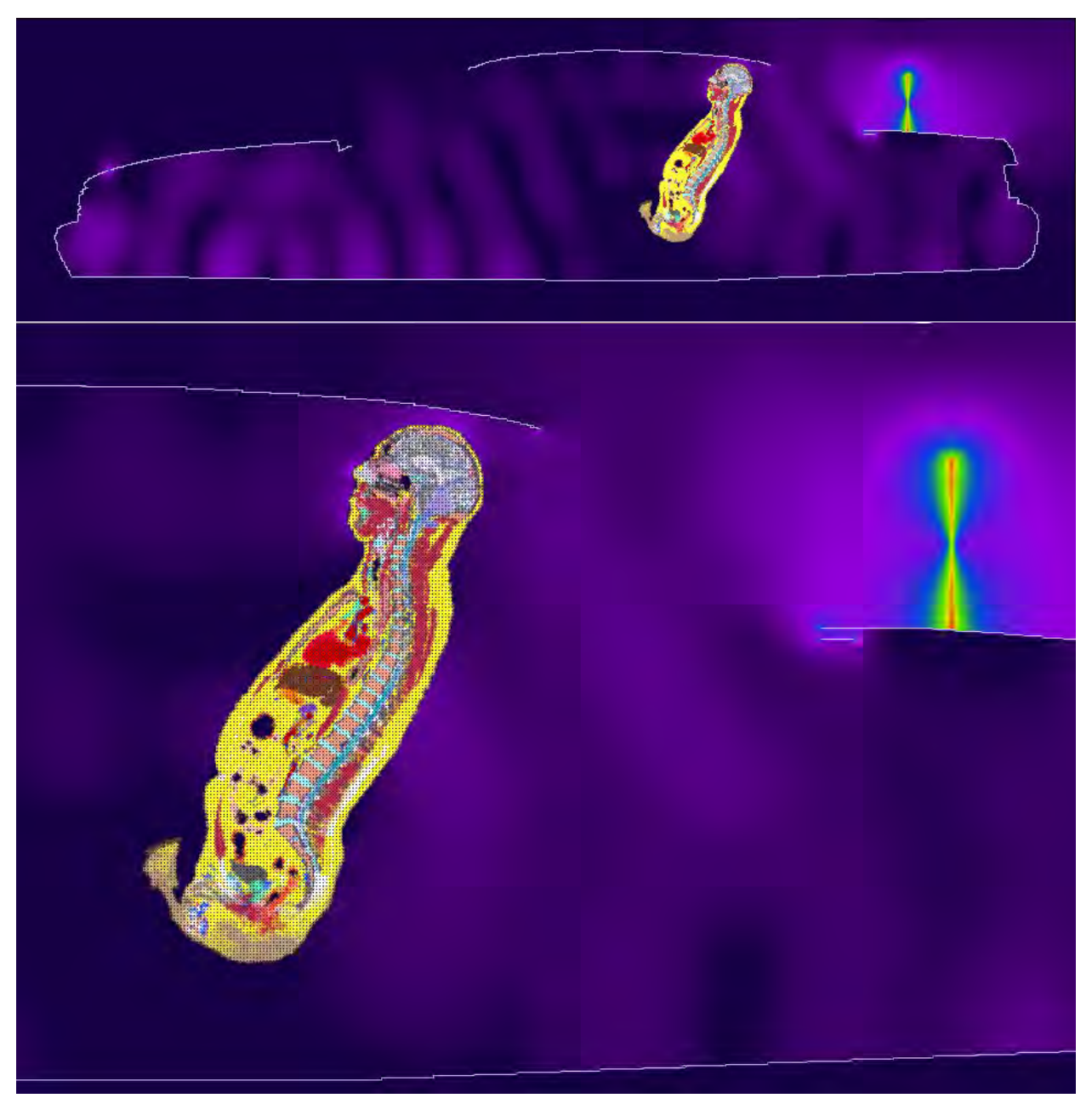


Figure 9. SAR distribution at 450.0125 MHz in the passenger model located on the center of the back seat, produced by the trunk-mount HAE6013A antenna. The contour plot is relative to the plane where the peak 1-g average SAR for this exposure condition occurs.

The pictures below in Figure 10 show the E and H field distributions in the plane of the antenna corresponding to the condition in Figure 9.



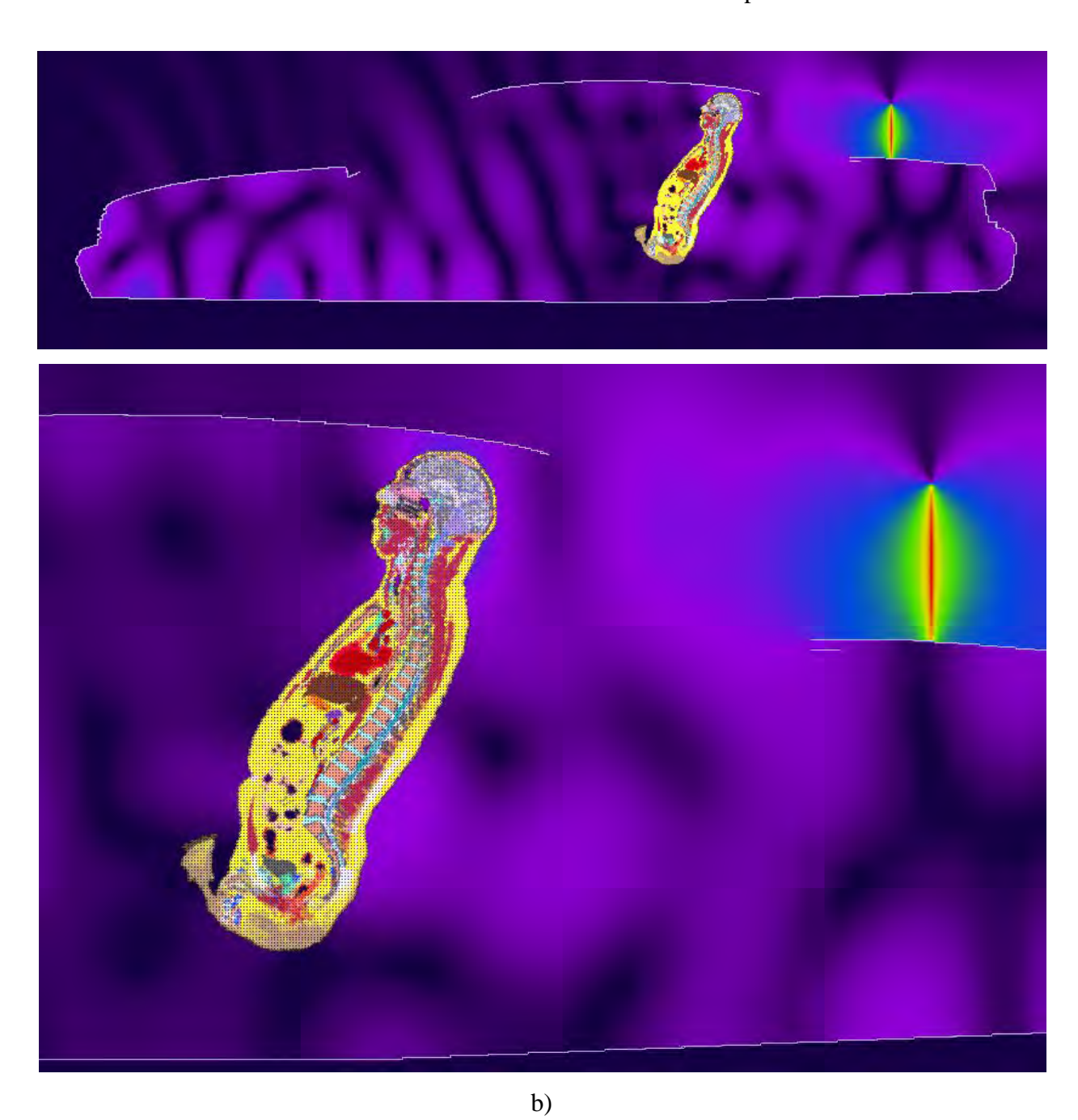


Figure 10. (a) E-field magnitude distribution corresponding to exposure condition of Figure 8, and (b) H-field magnitude distribution corresponding to exposure condition of Figure 8.

The highest adjusted 1-g SAR was produced in the passenger exposure condition with HAE6013A antenna at 450.0125 MHz (passenger on the center of the back seat).

#### **Results of SAR Computations**

FCC ID: AZ492FT7089/ ISED: 109U-92FT7089

The overall maximum peak 1-g SAR in all simulated conditions adjusted using the draft IEC/IEEE 62704-2 standard adjustment factor for VHF Band is 1.25 W/kg, UHF R1 Band is 1.39 W/kg, and UHF R2 Band is 0.96 W/kg, all less than the 1.6 W/kg limit, while the overall adjusted maximum peak 10-g SAR for VHF Band is 0.99 W/kg, UHF R1 Band is 1.07 W/kg, and UHF R2 Band is 0.67 W/kg, all less than the 2.0 W/kg limit. The adjusted maximum whole-body average SAR for VHF Band is 0.060 W/kg, UHF R1 Band is 0.05 W/kg, and UHF R2 Band is 0.05 W/kg, all less than the 0.08 W/kg limit.

#### **Conclusions**

Under the test conditions described for evaluating passenger exposure to the RF electromagnetic fields emitted by vehicle-mounted antennas used in conjunction with this mobile radio product, the present analysis shows that the computed SAR values are compliant with the FCC and ISED Canada exposure limits for the general public as well as with the corresponding ICNIRP and IEEE Std. C95.1-2005 SAR limits.

#### References

- [1] IEEE Standard C95.1-1999. *IEEE Standard for Safety Levels with Respect to Human Exposure to RF Electromagnetic Fields*, 3 kHz to 300 GHz.
- [2] http://www.nlm.nih.gov/research/visible/visible human.html
- [3] ICNIRP (International Commission on Non-Ionising Radiation Protection). 1998. Guidelines for limiting exposure to time-varying electric, magnetic and electromagnetic fields (up to 300 GHz). Health Phys. 74:494–522.
- [4] IEEE. 2005. IEEE standard for safety levels with respect to human exposure to radio frequency electromagnetic fields, 3 kHz to 300 GHz, IEEE Std C95.1-2005
- [5] Simon, W., Bit-Babik, G., "Effect of the variation in population on the whole-body average 1379 SAR of persons exposed to vehicle mounted antennas W. Simon", ICEAA September 2-7, 2012, Cape 1380 Town.

#### APPENDIX A: SPECIFIC INFORMATION FOR SAR COMPUTATIONS

This appendix follows the structure outlined in Appendix B.III of the Supplement C to the FCC OET Bulletin 65. Most of the information regarding the code employed to perform the numerical computations has been adapted from the draft IEC/IEEE 62704-1 and 62704-2 standards, and from the XFDTD<sup>TM</sup> User Manuals. Remcom Inc., owner of XFDTD<sup>TM</sup>, is kindly acknowledged for the help provided.

## 1) Computational resources

- a) A multiprocessor system equipped with two Intel Xeon E5-2697 v3 14-core CPUs and four NVIDIA Tesla K40 GPUs was employed for all simulations.
- b) The memory requirement was from 7 GB to 12 GB. Using the above-mentioned system with 8-cores operating concurrently, the typical simulation would run for 6-10 hours and with all four GPUs activated by the XFDTD version 7.3 this time would be from 60-180 min.

## 2) FDTD algorithm implementation and validation

a) We employed a commercial code (XFDTD<sup>TM</sup> v7.3, by Remcom Inc.) that implements the Yee's FDTD formulation [1]. The solution domain was discretized according to a rectangular grid with an adaptive 3-10 mm step in all directions. Sub-gridding was not used. Seven-layer PML absorbing boundary conditions are set at the domain boundary to simulate free space radiation processes. The excitation is a lumped voltage generator with 50-ohm source impedance. The code allows selecting wire objects without specifying their radius. We used a wire to represent the antenna. The car body is modeled by solid metal. We did not employ the "thin wire" algorithm since within the adaptive grid the minimum resolution of 3 mm was specified and used to model the antenna and the antenna wire radius was never smaller than onefifth of the voxel dimension. In fact, the XFDTD<sup>TM</sup> manual specifies that "In most cases, standard PEC material will serve well as a wire. However, in cases where the wire radius is important to the calculation and is less than 1/4 the length of the average cell edge, the thin wire material may be used to accurately simulate the correct wire diameter." The maximum voxel dimension in the plane normal to the antenna in all our simulations was 3 mm, and the antenna radius is always at least 1 mm (1 mm for the short quarter-wave antennas and 1.5 mm for the long gain antennas), so there was no need to specify a "thin wire" material.

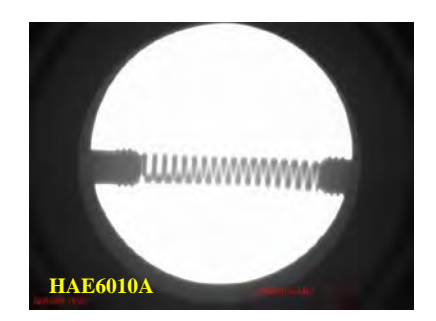
Because the field impinges on the bystander or passenger model at a distance of several tens of voxels from the antenna, the details of antenna wire modeling are not expected to have significant impact on the exposure level.

Some antennas have inductive loading coils located in the mid section as shown in the picture below of the HAE 6010A and HAE 4011A antenna examples.



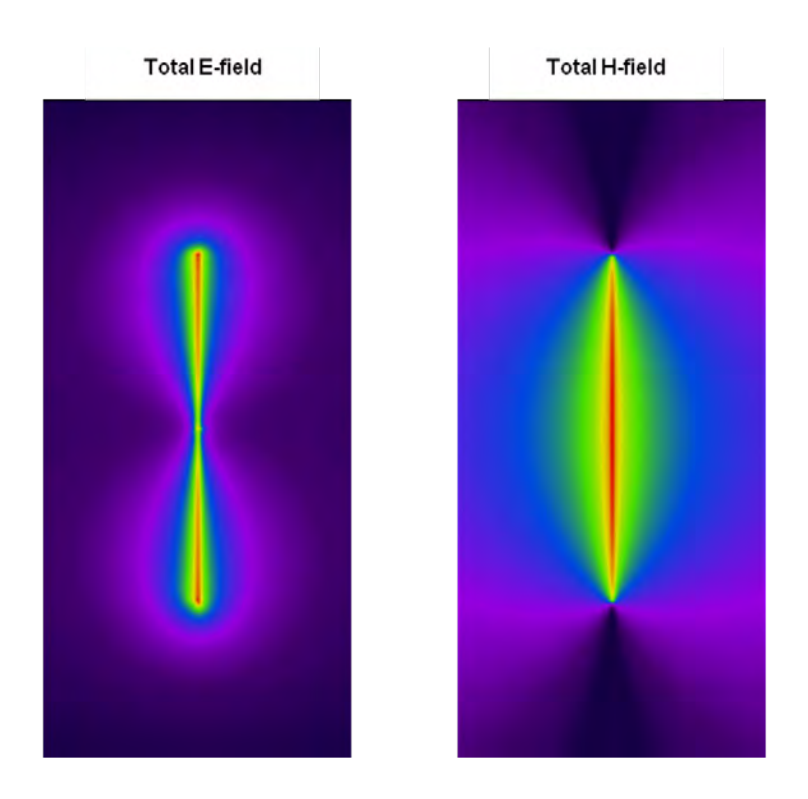
The X-ray of the reactive loads of the HAE4011A and HAE6010A antennas is also presented in the next pictures below. Those elements are significantly shorter than the length of the antenna and are about 1/40 of the wavelength at center operating frequency. They were modeled as lumped reactive elements. The comparison with measurements and validity of such simulation model has been summarized in [9].

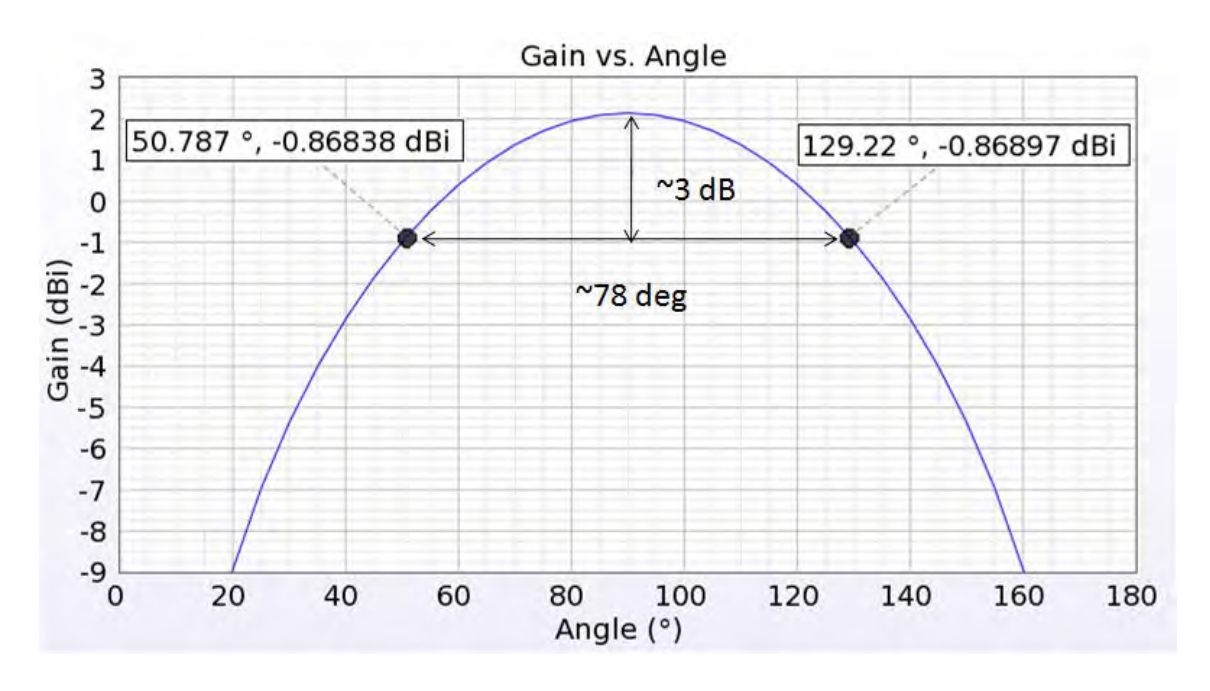




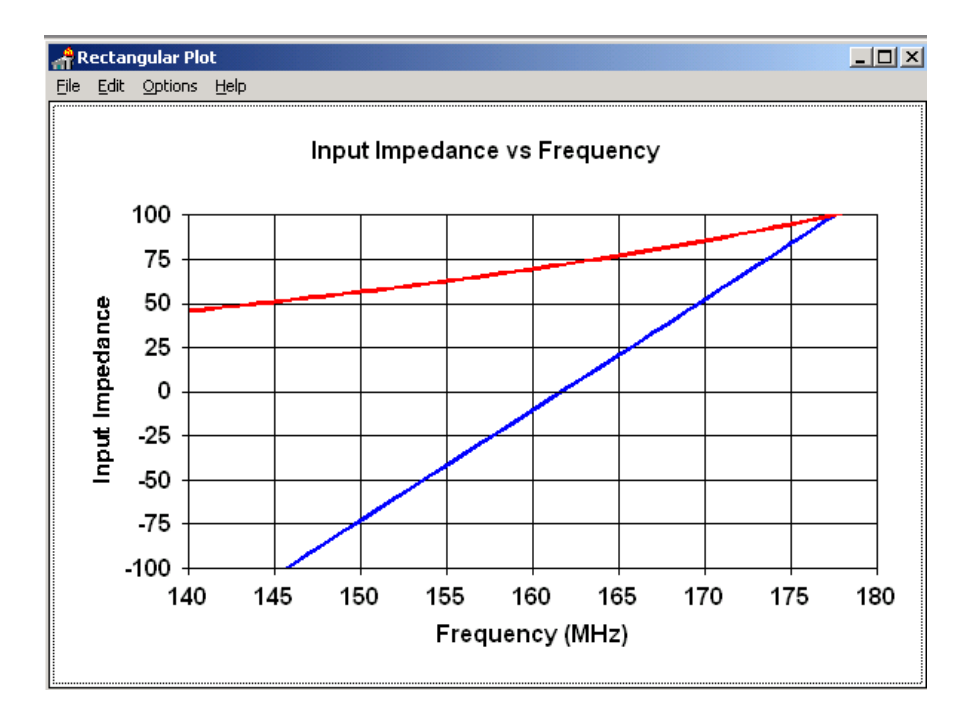
b) XFDTD™ is one of the most widely employed commercial codes for electromagnetic simulations. It has gone through extensive validation and has proven its accuracy over time in many different applications. One example is provided in [3].

We carried out a validation of the code algorithm by running the canonical test case involving a half-wave wire dipole. The dipole is 0.475 times the free space wavelength at 160 MHz, i.e., 88.5 cm long. The discretization used to model the dipole was 5 mm. Also in this case, the "thin wire" model was not needed. The following picture shows XFDTD<sup>TM</sup> outputs regarding the antenna feed-point impedance (70.5 - j 6.0 ohm), as well as qualitative distributions of the total E and H fields near the dipole. The radiation pattern is shown as well (one lobe in elevation). As expected, the 3 dB beamwidth is about 78 degrees.

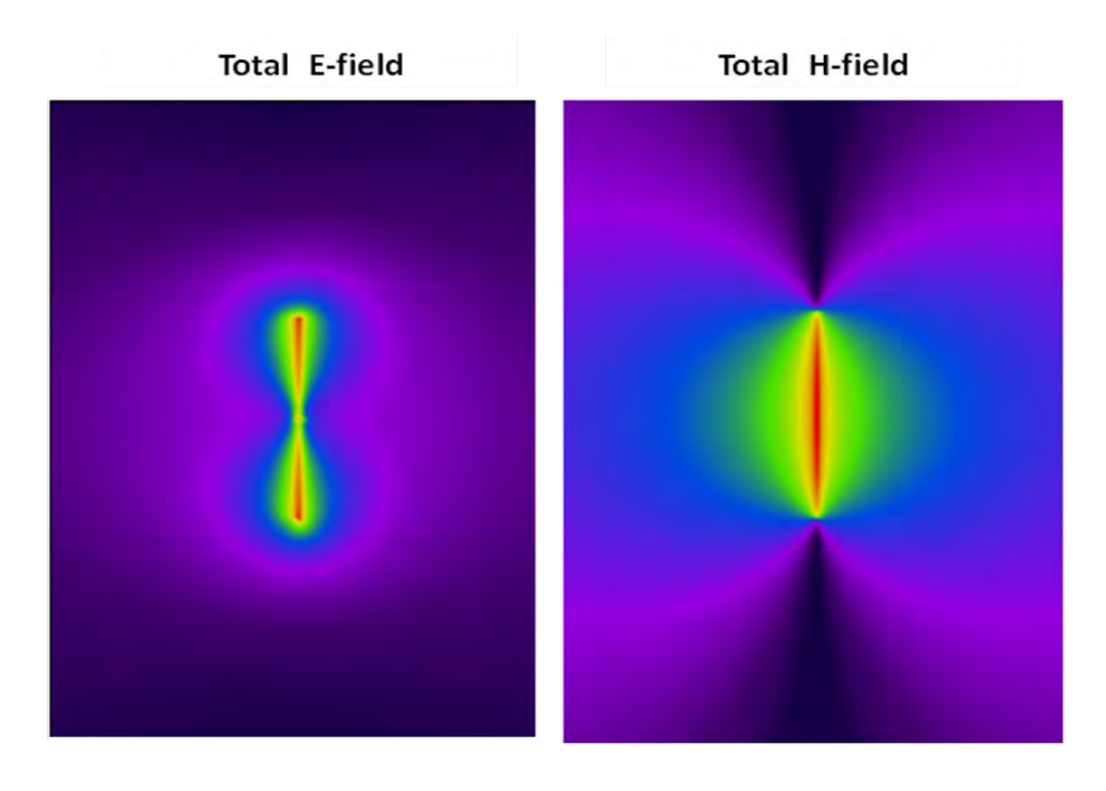


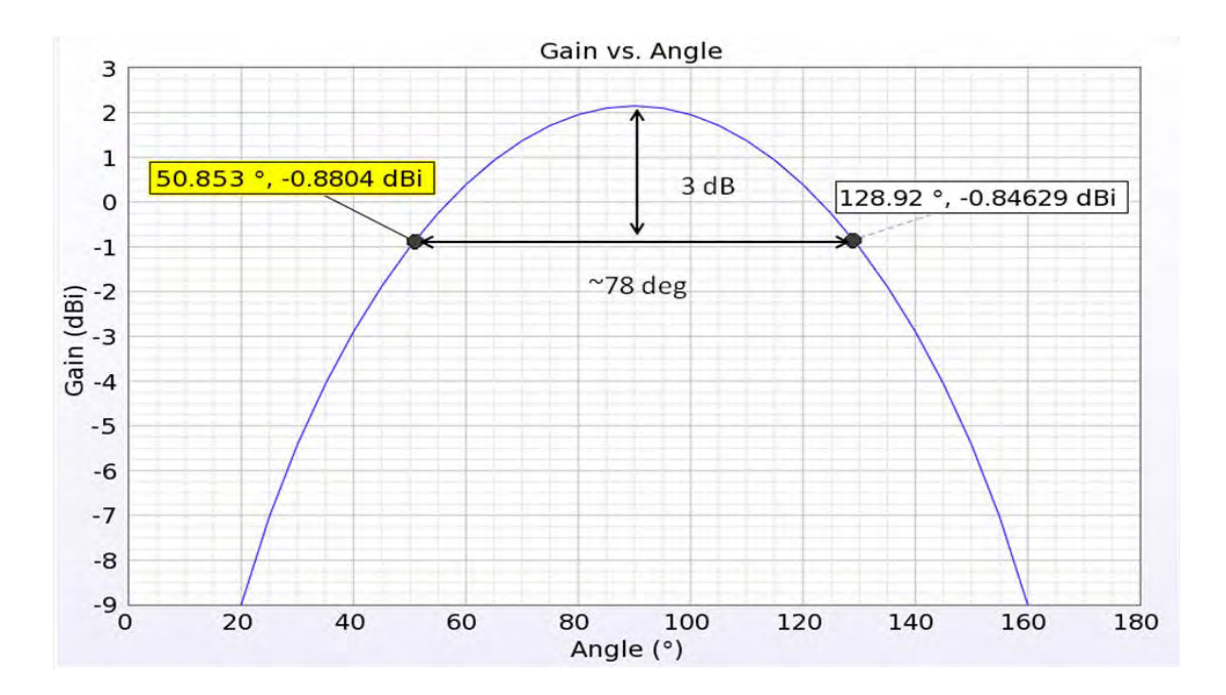


We also compared the XFDTD<sup>TM</sup> result with the results derived from NEC [4], which is a code based on the method of moments. In this case, we used a dipole with radius 1 mm, length 88.5 cm, and the discretization is 5 mm. The corresponding input impedance at 160 MHz is 69.5-j10.5 ohm. Its frequency dependence is reported in the following figure.



We also carried out similar validation at 400 MHz, i.e., about 35.5 cm long. The following picture shows XFDTD<sup>TM</sup> outputs regarding the antenna feed-point impedance (75.5 + j 11.9 ohm), as well as qualitative distributions of the total E and H fields near the dipole. The radiation pattern is shown as well (one lobe in elevation). As expected, the 3 dB beamwidth is about 78 degrees in this case as well. The computed results are in good agreement with the known analytical results for the half -wave dipole antenna which could be found in [10].





This validation ensures that the input impedance calculation is carried out correctly in XFDTD<sup>TM</sup>, thereby enabling accurate estimates of the radiated power. It further ensures that the wire model employed in XFDTD<sup>TM</sup>, which we used to model the antennas, produces physically meaningful current and fields distributions. Both these aspects ensure that the field quantities are correctly computed both in terms of absolute amplitude and relative distribution.

# 3) Computational parameters

a) The following table reports the main parameters of the FDTD model employed to perform our computational analysis:

PARAMETER	X	Y	Z	
Voxel size	3-9 mm	3-9 mm	1-9 mm	
Maximum domain dimensions employed for passenger computations (cells)	479	1035	671	
Maximum domain dimensions employed for bystander computations (cells)	936	992	780	
Time step	About 0.7 of the C	Courant limit (ty	pically 5 ps)	
Objects separation from FDTD boundary (mm)	>200	>200	>200	
Number of time steps	Defined to reach -60 dB convergence			
Excitation	Sinusoidal (not less than 10 periods)			

# 4) Phantom model implementation and validation

a) The human body models (bystander and/or passenger) employed in our simulations are those defined in the draft IEC/IEEE 62704-2 standard. They are originally derived from data of the *visible human project* sponsored by the National Library of Medicine (NLM)

(http://www.nlm.nih.gov/research/visible/visible\_human.html). The original male data set consists of MRI, CT and anatomical images. Axial MRI images of the head and neck and longitudinal sections of the rest of the body are available at 4 mm intervals. The MRI images have 256 pixel by 256 pixel resolution. Each pixel has 12 bits of gray tone resolution. The CT data consists of axial CT scans of the entire body taken at 1 mm intervals at a resolution of 512 pixels by 512 pixels where each pixel is made up of 12 bits of gray tone. The axial anatomical images are 2048 pixels by 1216 pixels where each pixel is defined by 24 bits of color. The anatomical cross sections are also at 1 mm intervals and coincide with the CT axial images. There are 1871 cross sections. Dr. Michael Smith and Dr. Chris Collins of the Milton S. Hershey Medical Center, Hershey, Pa, created the High Fidelity Body mesh. Details of body model creation are given in the *methods* section in [5].

The final bystander and passenger model was generated for the IEC/IEEE 62704-2 standard from the above dataset using the Varipose softwar, Remocm Inc., The body mesh contains 39 tissues materials. Measured values for the tissue parameters for a broad frequency range are included with the mesh data. The correct values are interpolated from the table of measured data and entered into the appropriate mesh variables. The tissue conductivity and permittivity variation *vs.* frequency is included in the XFDTD<sup>TM</sup> calculation by a multiple-pole approximation to the Cole-Cole approximated tissue parameters reported in [11].

- a) The XFDTD<sup>TM</sup> High Fidelity Body Mesh model correctly represents the anatomical structure and the dielectric properties of body tissues, so it is appropriate for determining the highest exposure expected for normal device operation.
- b) One example of the accuracy of XFDTD<sup>™</sup> for computing SAR has been provided in [6]. The study reported in [6] is relative to a large-scale benchmark of measurement and computational tools carried out within the IEEE Standards Coordinating Committee 34, Sub-Committee 2.

#### 5) Tissue dielectric parameters

Tissue dielectric parameters were defined as specified in the IEEE/IEC 62704-2 draft standard. XFDTD code implements the related formulation for dielectric constant and conductivity and automatically adjust the values according to the specified frequency.

a) The following table reports the dielectric properties computed for the 39 body tissue materials in the employed human body models at 150 MHz as an example.

#	Tissue	$\epsilon_{ m r}$	σ (S/m)	Density (kg/m³)
1	bile	85.3	1.60	928
2	body fluid	71.3	1.26	1050
3	eye cornea	69.0	1.07	1051
4	fat	12.2	0.07	911
5	lymph	65.7	0.81	1035
6	mucous membrane	59.2	0.56	1102
7	toe, finger, and nails	14.4	0.07	1908
8	nerve spine	42.3	0.36	1075
9	muscle	62.2	0.73	1090
10	heart	80.7	0.79	1081
11	white matter	50.3	0.35	1041
12	stomach	73.3	0.92	1088
13	glands	65.7	0.81	1028
14	blood vessel	54.0	0.49	1102
15	liver	61.7	0.53	1079
16	gall bladder	71.3	1.06	1071
17	spleen	78.8	0.86	1089
18	cerebellum	74.6	0.85	1045
19	cortical bone	14.4	0.07	1908
20	cartilage	51.4	0.50	1100
21	ligaments	50.8	0.50	1142
22	skin	61.5	0.54	1109
23	large intestine	73.8	0.72	1088
24	tooth	14.4	0.07	2180
25	grey_matter	70.1	0.60	1045
26	eye lens	41.7	0.32	1076
27	outer lung	61.9	0.59	1050
28	small intestine	83.4	1.72	1030
29	eye sclera	63.5	0.93	1032
30	innerlung	28.3	0.32	394
31	pancreas	65.7	0.81	1087
32	blood	71.3	1.26	1050
33	cerebro_spinal_fluid	81.2	2.16	1007
34	eye vitreoushumor	69.1	1.51	1005
35	kidneys	85.0	0.88	1066
36	bone marrow	13.2	0.16	1029
37	bladder	21.4	0.30	1086
38	testicles	70.3	0.94	1082
39	cancellous bone	25.5	0.19	1178

The following table also reports the dielectric properties computed for the 39 body tissue materials in the employed human body models at 450 MHz as an example.

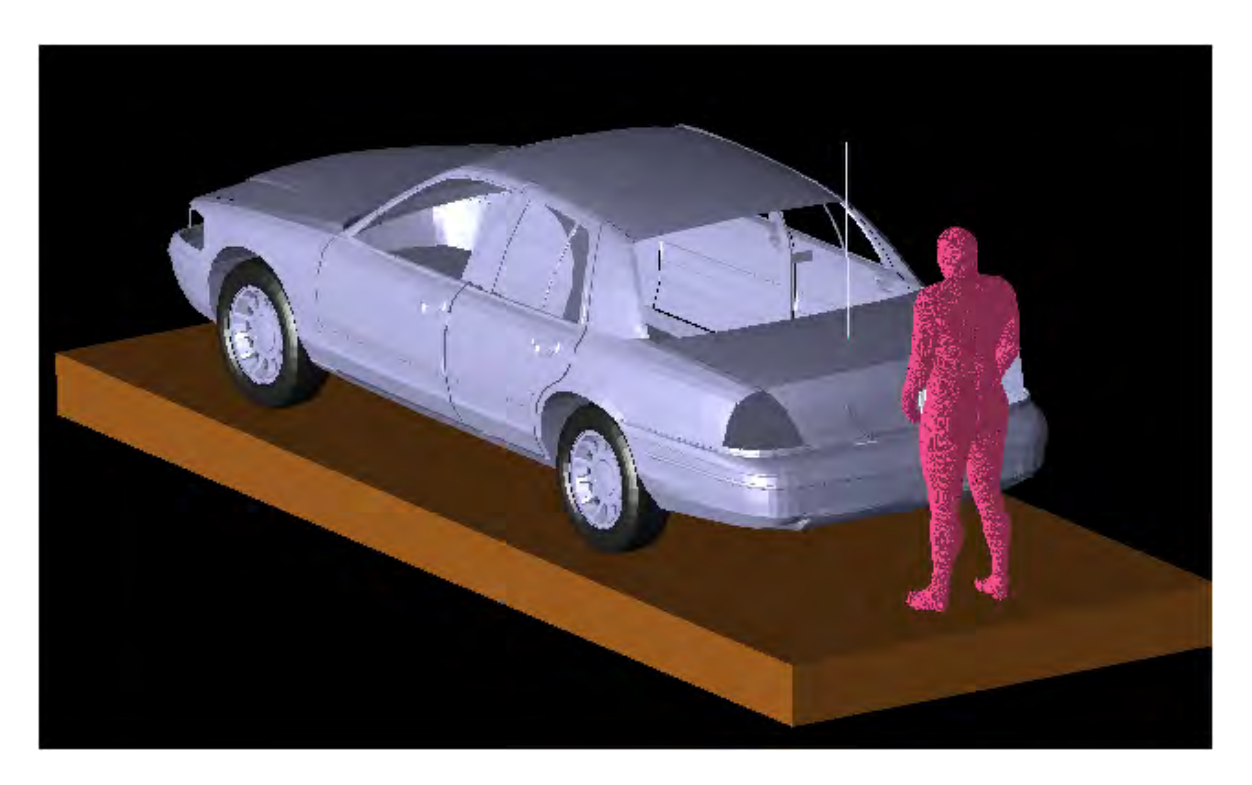
#	Tissue	ε <sub>r</sub>	σ (S/m)	Density (kg/m³)
1	bile	72.2	1.71	928
2	body fluid	63.7	1.37	1050
3	eye cornea	58.5	1.21	1051
4	fat	11.6	0.08	911
5	lymph	61.2	0.89	1035
6	mucous membrane	49.2	0.69	1102
7	toe, finger, and nails	13.0	0.10	1908
8	nerve spine	34.9	0.46	1075
9	muscle	56.8	0.81	1090
10	heart	65.0	0.99	1081
11	white matter	41.5	0.46	1041
12	stomach	67.1	1.02	1088
13	glands	61.2	0.89	1028
14	blood vessel	46.6	0.57	1102
15	liver	50.4	0.67	1079
16	gall bladder	60.7	1.15	1071
17	spleen	62.1	1.05	1089
18	cerebellum	54.7	1.06	1045
19	cortical bone	13.0	0.10	1908
20	cartilage	45.0	0.60	1100
21	ligaments	47.0	0.57	1142
22	skin	45.8	0.71	1109
23	large intestine	61.7	0.88	1088
24	tooth	13.0	0.10	2180
25	grey_matter	56.6	0.76	1045
26	eye lens	37.2	0.38	1076
27	outer lung	54.0	0.70	1050
28	small intestine	64.9	1.93	1030
29	eye sclera	57.2	1.02	1032
30	innerlung	23.5	0.38	394
31	pancreas	61.2	0.89	1087
32	blood	63.7	1.37	1050
33	cerebro_spinal_fluid	70.5	2.26	1007
34	eye vitreoushumor	69.0	1.54	1005
35	kidneys	65.0	1.13	1066
36	bone marrow	11.8	0.19	1029
37	bladder	19.6	0.33	1086
38	testicles	62.9	1.04	1082
39	cancellous bone	22.2	0.24	1178

- b) The tissue types and dielectric parameters used in the SAR computation are appropriate for determining the highest exposure expected for normal device operation, because they are derived from measurements performed on real biological tissues and are also defined in the computational draft standard IEC/IEEE 62704-2.
- c) The tabulated list of the dielectric parameters used in phantom models is provided at point 5(a). As regards the device (car plus antenna), we used perfect electric conductors.

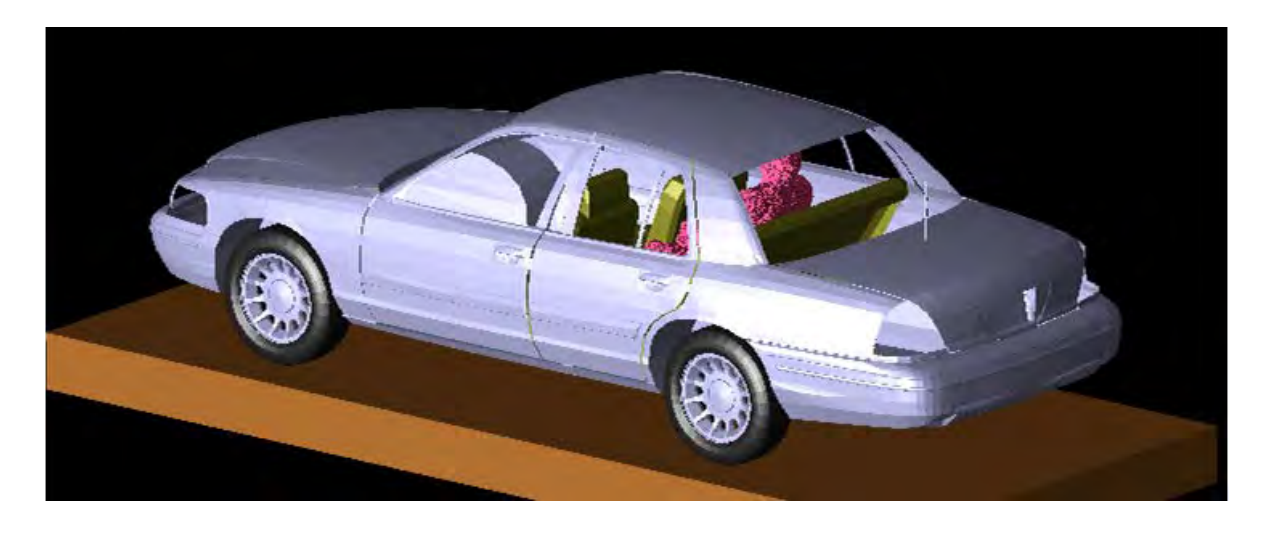
#### 6) Transmitter model implementation and validation

- a) The essential features that must be modeled correctly for the particular test device model to be valid are:
  - Car body. The standard car model developed and defined in the SAR computational draft standard IEC/IEEE 62704-2 has been employed in simulations.
  - Antenna. We used a straight wire, even when the gain antenna has a base coil for tuning. All the coil does is compensating for excess capacitance due to the antenna being slightly longer than half a wavelength. We do not need to do that in the model, as we used normalization with respect to the net radiated power, which is determined by the input resistance only. In this way, we neglect mismatch losses and artificially produce an overestimation of the SAR, thereby introducing a conservative bias in the model. This simulation model was also validated by comparing the computed and measured near-field distributions in the condition with antenna mounted on the reference ground plane and showed good agreement experimental data [9].
  - Antenna location. We used the same location, relative to the edge of the car trunk, the backseat, or the roof, used in the MPE measurements. The following pictures show a lateral and a perspective view of the bystander and passenger model.









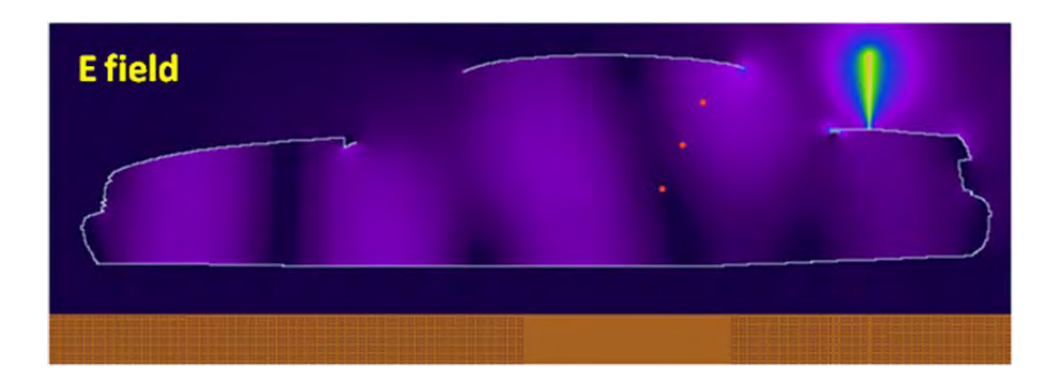
The car model is constituted by perfect electric conductor and does not include wheels in order to reduce its complexity. The passenger model is surrounded by air, as the seat, which is made out of poorly conductive fabrics, is not included in the computational model. The pavement has not been included in the model. The passenger and bystander models were validated for similar antenna and frequency conditions by comparing the MPE measurements at two VHF frequencies (146 MHz and 164 MHz) for antennas used for a VHF mobile radio analyzed previously in 2003 (FCC ID#ABZ99FT3046). The corresponding MPE measurements are reported in the compliance report relative to FCC ID#ABZ99FT3046. The comparison results are presented below, according to following definitions for the equivalent power densities (based on E or H-field):

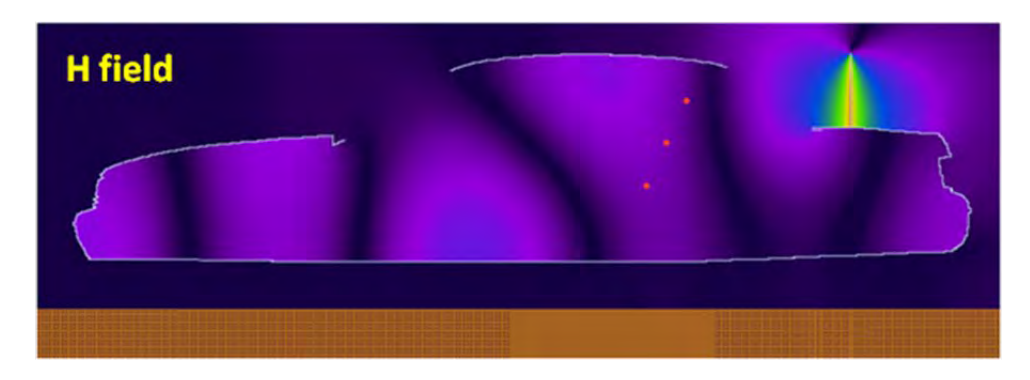
$$S_E = \frac{\left|\mathbf{E}\right|^2}{2\eta}, \quad S_H = \frac{\eta}{2}\left|\mathbf{H}\right|^2, \quad \eta = 377 \ \Omega.$$

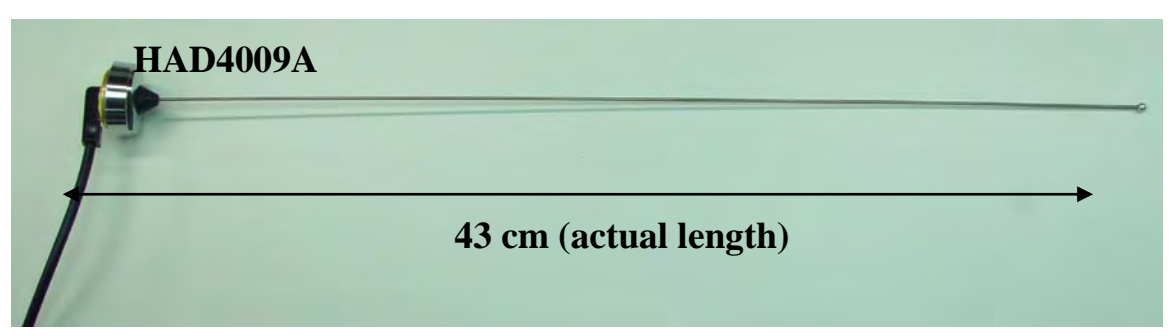
The mobile radios used for these validations had different output power levels depending on the radio model and frequency as described in each validation case below. However, the fact that this power is different from the output power of the current device under test is irrelevant since the field probe used during the validation measurements was always operating within its stated operating range.

# Passenger with 43 cm monopole antenna (HAD4009A 164 MHz)

The following figures of the test model show the empty car model, where the red dotted line represents the location of the passenger in the back seat, as it can be observed from the complete model picture above. The comparison has been performed by taking the computed steady-state field values at the red dots locations corresponding to the head, chest, and lower trunk area and comparing them with the corresponding measurements. Such a comparison is carried out at the same average power level (56.5 W) used in the measurements. Steady-state E-field and H-field distributions at a vertical crossing the passenger's head are displayed as well. Finally, a picture of the antenna is shown.

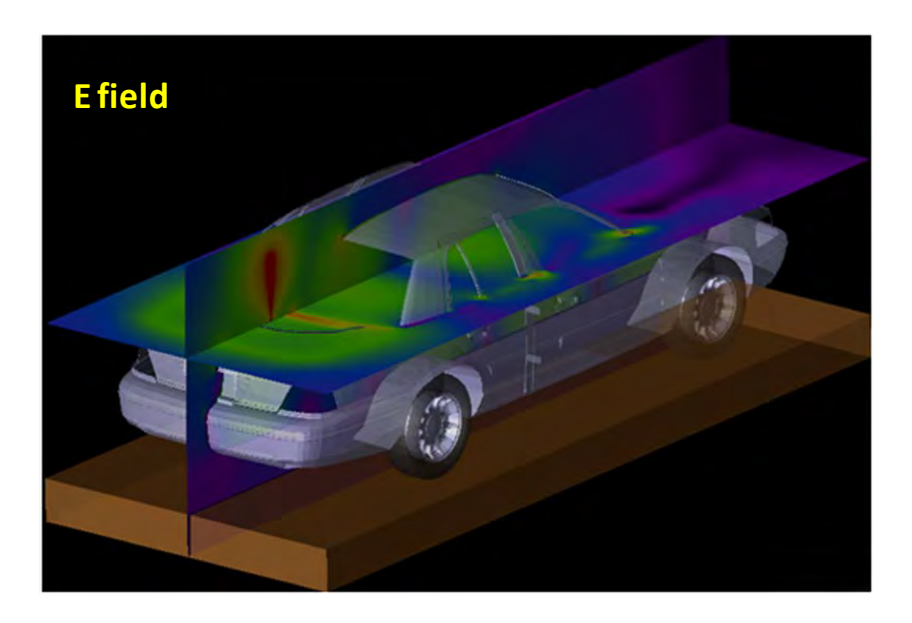


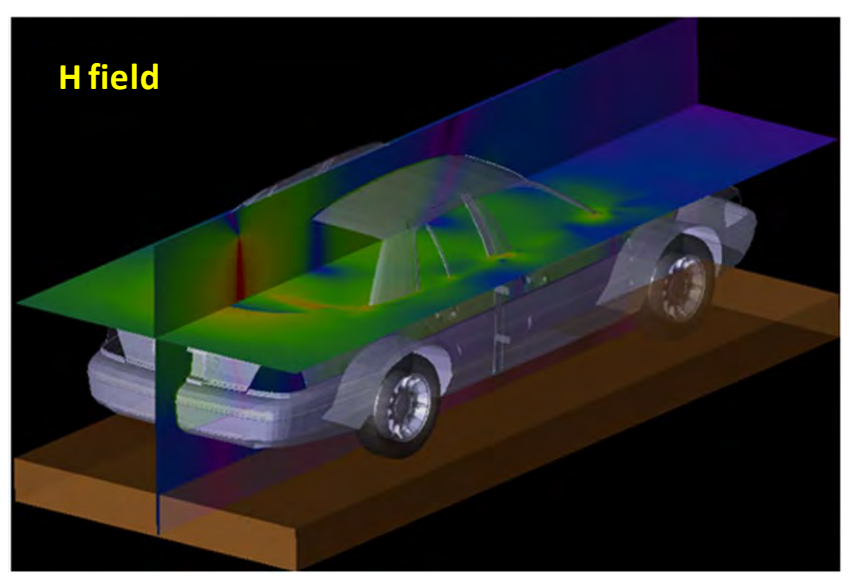




The highest exposure occurs in the middle of the backseat, which is also the case in the measurements. Therefore, the field values were determined on the yellow line centered at the middle of the backseat, approximately at the three locations that are shown by white dots. In actuality, the line is inclined so as to follow the inclination of the passenger's back, as shown previously.

Because the peak exposure occurs in the center of the back seat, that was where we placed the passenger model to perform the SAR evaluations presented in the report. However, it can be observed that the H-field distribution features peaks near the lateral edges of the rear window. That is the reason why we also carried out one SAR computation by placing the passenger laterally in the back seat, in order to determine whether the SAR would be higher in this case.





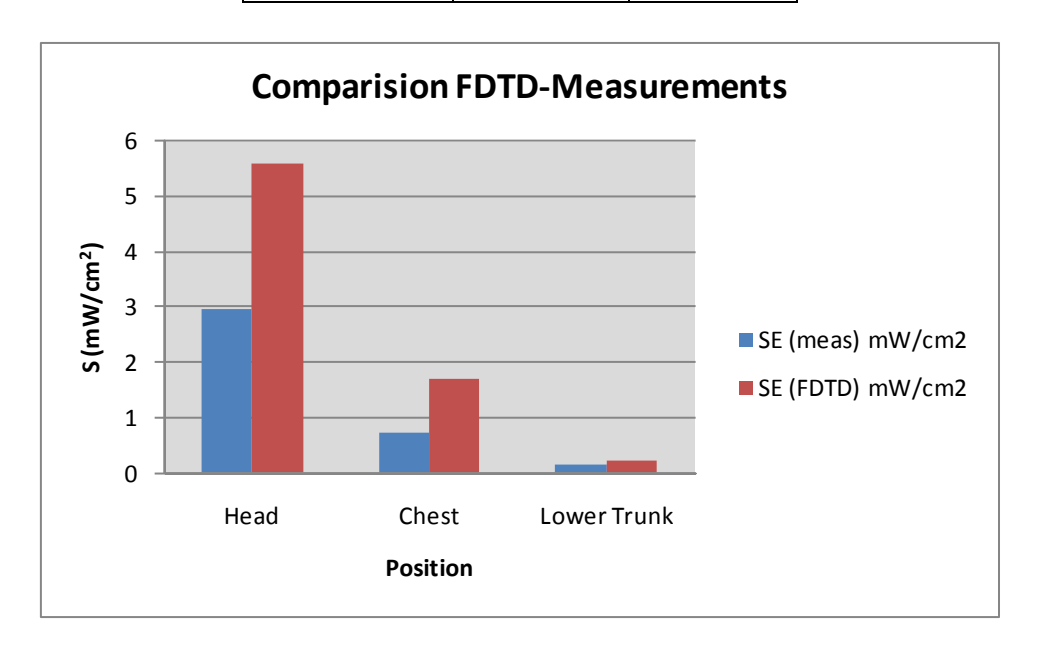
As done in the measurements, the equivalent power density (S) is computed from the E-field, the H-field being much lower. The following table reports the E-field values computed by XFDTD<sup>TM</sup> at the three locations, and the corresponding power density.

Location	E-field magnitude (V/m)	$S(W/m^2)$
Head	1.27	2.14E-03
Chest	0.70	6.55E-04
Lower Trunk area	0.20	7.70E-05
	Average S	9.57E-04

The input impedance is 24.8-j11.9 ohm, therefore the radiated power (considering the mismatch to the 50 ohm unitary voltage source) is 2.16E-3 W. The scaled-up power density for 56.5 W radiated power is  $25.0 \text{ W/m}^2$ , corresponding to  $2.50 \text{ mW/cm}^2$ . Measurements gave an average of

1.29 mW/cm<sup>2</sup>, which is a reasonable overestimation considering conservativeness of simulations model. The following table and the graph show a comparison between the simulated power density and the measured one (see also MPE report in FCC ID#ABZ99FT3046, Table 43), normalized to 56.5 W radiated.

Position	SE (meas) mW/cm <sup>2</sup>	SE (FDTD) mW/cm <sup>2</sup>
Head	2.98	5.59
Chest	0.74	1.71
Lower Trunk	0.14	0.2

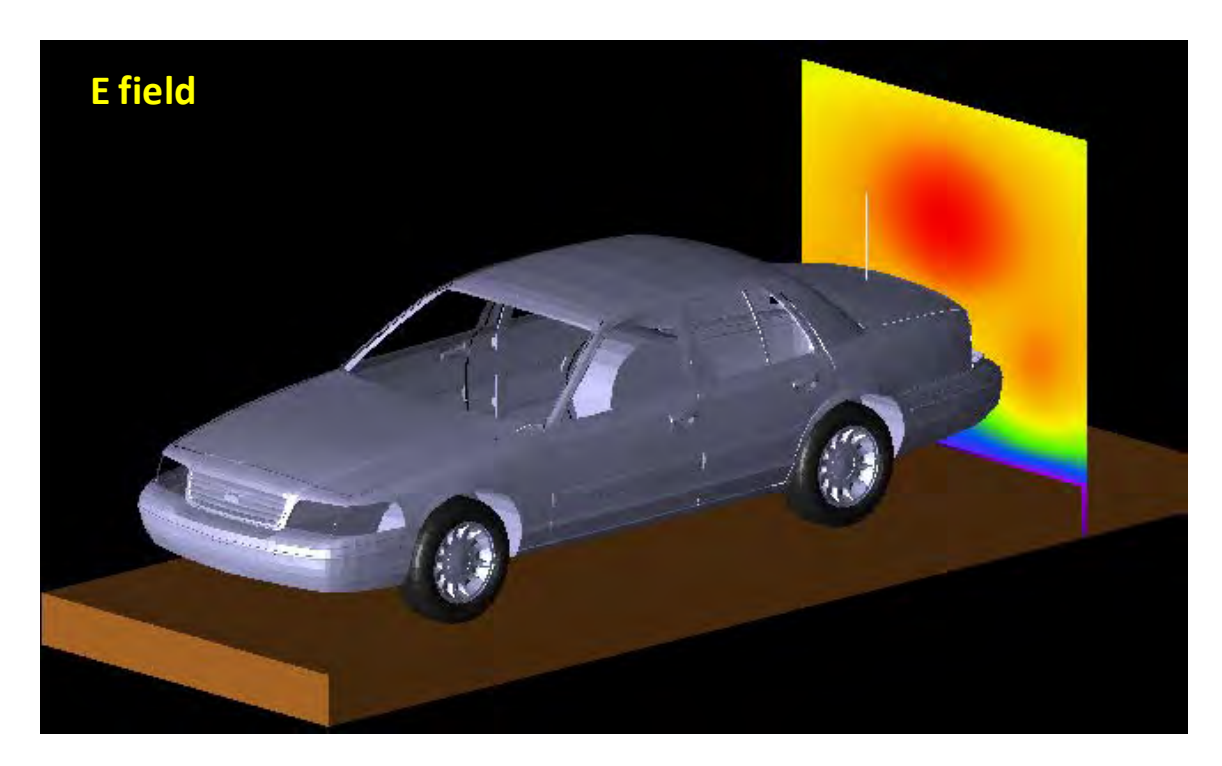


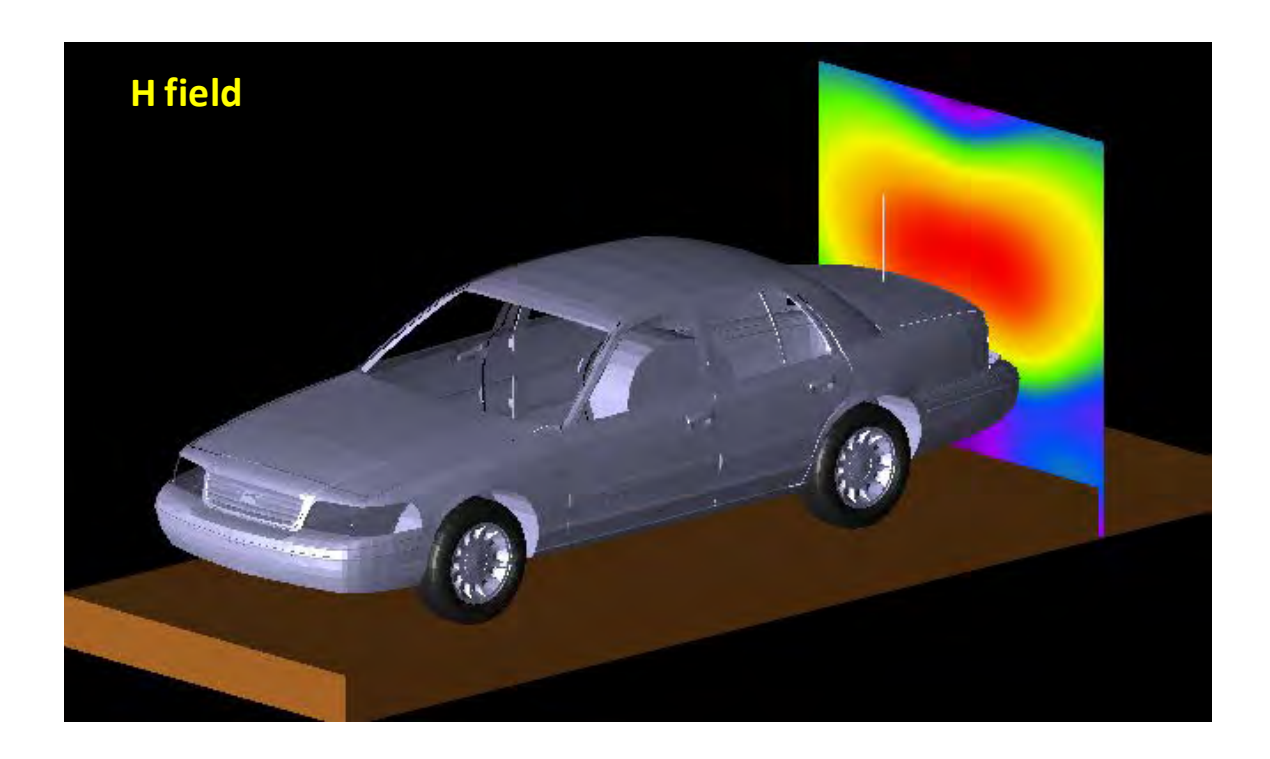
# Bystander with 48 cm monopole antenna (HAD4007A 146 MHz)

The following figures show the E-field and H-field distributions across a vertical plane passing for the antenna and cutting the car in half. As done in the measurements, the MPE is computed from both E-field and H-field distributions, along the yellow dotted line at 10 points spaced 20 cm apart from each other up to 2 m in height. These lines and the field evaluation points are approximately indicated in the figures. The E-field and H-field distributions in the vertical plane placed at 60 cm from the antenna, are shown as well. The points where the fields are sampled to determine the equivalent power density (S) are approximately indicated by the white dots. A picture of the antenna is not reported because it is identical to the HAD4009A except for the length.







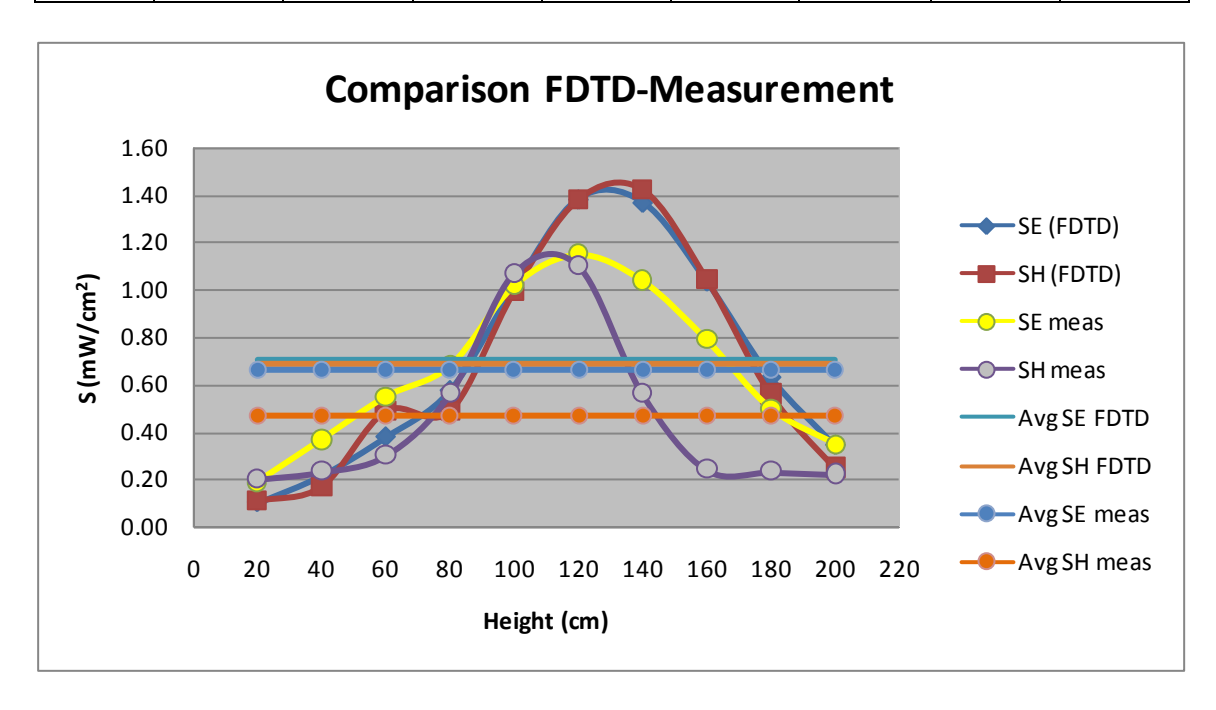


The following table reports the field values computed by XFDTD<sup>TM</sup> and the corresponding power density values. The average exposure levels are computed as well.

Height (cm)	E (V/m)	$S_{\rm E} (W/m^2)$	H (A/m)	$S_{\rm H} (W/m^2)$
20	1.84E-01	4.50E-05	5.10E-04	4.89E-05
40	2.71E-01	9.71E-05	6.38E-04	7.68E-05
60	3.58E-01	1.70E-04	1.08E-03	2.20E-04
80	4.42E-01	2.59E-04	1.54E-03	2.20E-04
100	5.85E-01	4.55E-04	1.82E-03	4.48E-04
120	6.86E-01	6.24E-04	1.85E-03	6.23E-04
140	6.82E-01	6.17E-04	1.58E-03	6.42E-04
160	5.93E-01	4.67E-04	1.16E-03	4.72E-04
180	4.63E-01	2.84E-04	7.67E-04	2.52E-04
200	3.41E-01	1.55E-04	4.94E-04	1.11E-04
	Average $S_E$	3.17E-04	Average S <sub>H</sub>	3.11E-04

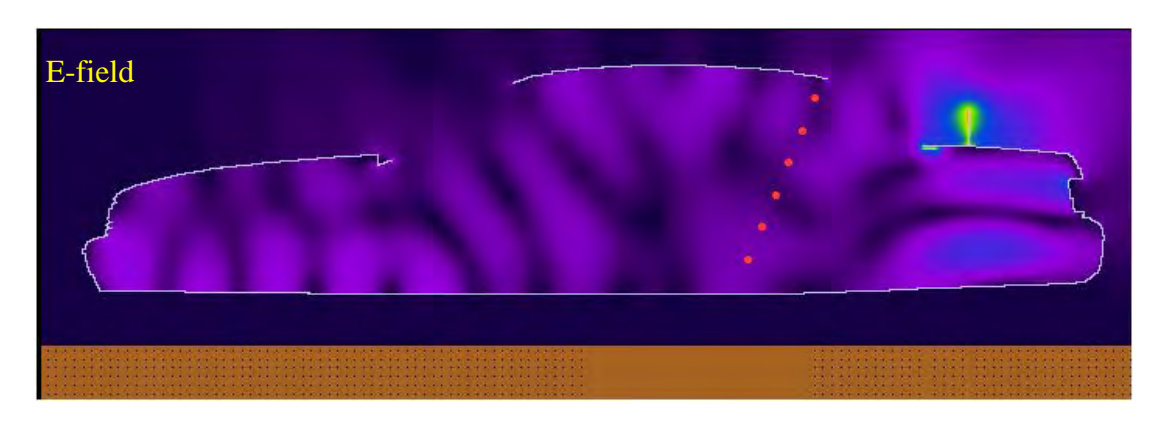
The input impedance is 33.7-j3.0 ohm, therefore the radiated power (considering the mismatch to the 50 ohm unitary voltage source) is 2.40E-3 W. The scaled-up power density values for 53.2 W radiated power are 7.03 W/m $^2$  (E), and 6.90 W/m $^2$  (H), that correspond to 0.70 mW/cm $^2$  (E), and 0.69 mW/cm $^2$  (H). Measurements yielded average power density of 0.664 mW/cm $^2$  (E), and 0.471 mW/cm $^2$  (H), i.e., which are in good agreement with the simulations. The following table and graph show a comparison between the simulated power density and the measured one, based on E (see MPE report in FCC ID#ABZ99FT3046, Table 1) or H fields (see MPE report in FCC ID#ABZ99FT3046, Table 13), normalized to 53.2 W radiated.

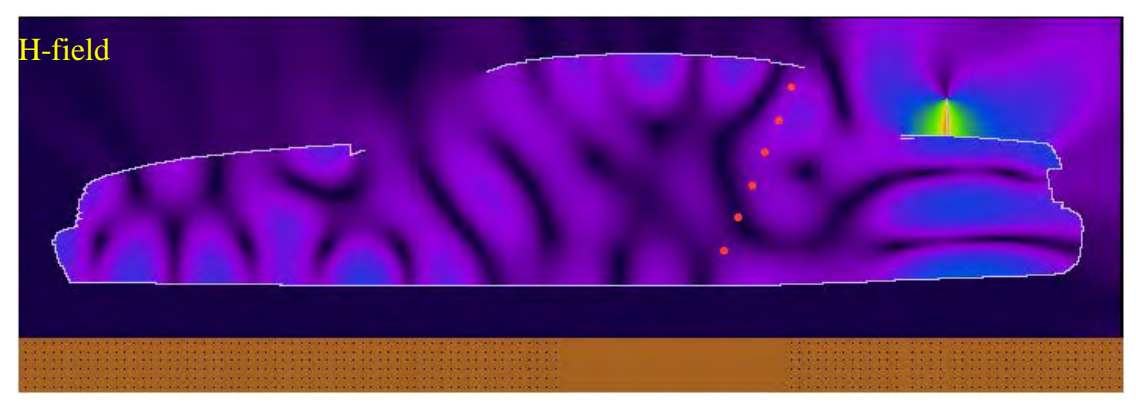
Height (cm)	SE (meas) mW/cm <sup>2</sup>	SE (FDTD) mW/cm <sup>2</sup>	SH (meas) mW/cm <sup>2</sup>	SH (FDTD) mW/cm <sup>2</sup>	Avg SE meas mW/cm <sup>2</sup>	Avg SE FDTD mW/cm <sup>2</sup>	Avg SH meas mW/cm <sup>2</sup>	Avg SH FDTD mW/cm <sup>2</sup>
20	0.19	0.10	0.2	0.11				
40	0.37	0.22	0.23	0.17				
60	0.55	0.38	0.3	0.49				
80	0.68	0.57	0.56	0.49				
100	1.02	1.01	1.07	0.99	0.664	0.703	0.471	0.690
120	1.15	1.38	1.1	1.38	0.004	0.703	0.471	0.090
140	1.04	1.37	0.56	1.42				
160	0.79	1.03	0.24	1.05				
180	0.5	0.63	0.23	0.56				
200	0.35	0.34	0.22	0.25				

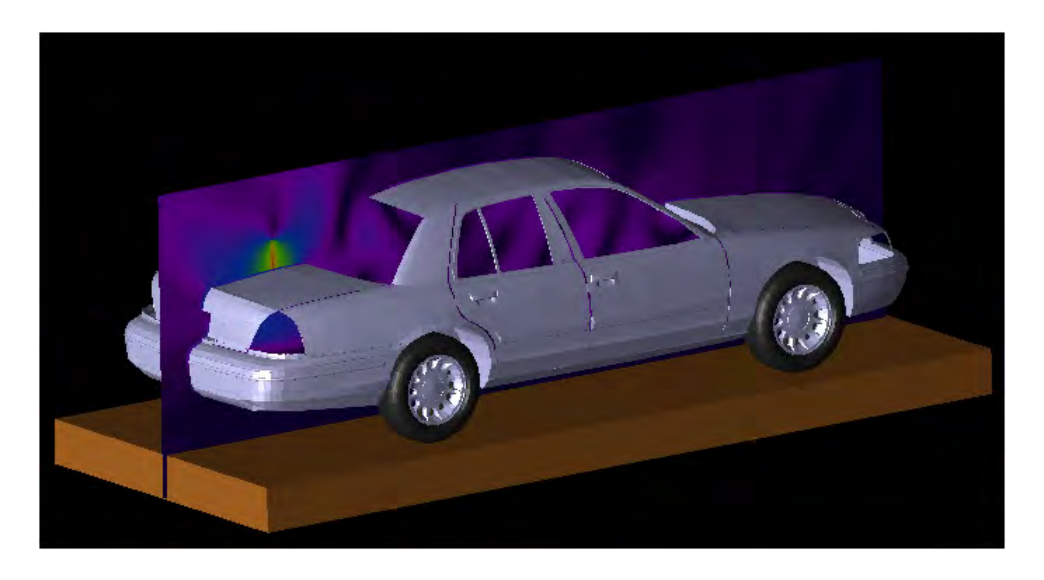


#### Passenger with 17.5 cm monopole antenna (HAE4002A 421.5 MHz)

The following figure of the test model shows the car model, where the red dots individuate the back seat, as it can be observed from the other figure showing the cross section of the passenger. The comparison has been performed by taking the average of the computed steady-state field values at the six dotted locations, corresponding to the head, chest, and legs along the red dots line, and comparing them with the average of the MPE measurements performed at the head, chest and legs locations. Such a comparison is carried out at the same average power level (22 W, including the 50% duty factor) used in the MPE measurements.







The equivalent power density (S) is computed from the E-field and the H-field separately. The following table reports the E-field values computed by XFDTD<sup>TM</sup> at the six locations, and the corresponding power density.

Locatio	E-field,	Eq. Power	Scaled			
n	V/ m	Density 1.0	Power Dens.			
Number		V source	22 W			
			out put ,			
			mW/cm^2			
1	3.11E-01	1.28E-04	1.56E-01			
2	4.16E-01	2.29E-04	2.79E-01			
3	5.25E-01	3.65E-04	4.45E-01			
4	3.86E-01	1.98E-04	2.41E-01			
5	3.84E-01	1.96E-04	2.39E-01			
6	6.01E-01	4.80E-04	5.85E-01			
Equivalent average Power Density 3.24E-01						

Locatio	H-field,	Eq. Power	Scaled			
n	Weber/ m2	Density 1.0	Power Dens.			
Number		V source	22 W			
			out put ,			
			mW/cm^2			
1	1.34E-03	3.37E-04	4.11E-01			
2	1.08E-03	2.21E-04	2.70E-01			
3	5.59E-04	5.89E-05	7.18E-02			
4	5.45E-04	5.60E-05	6.82E-02			
5	5.45E-04	5.59E-05	6.82E-02			
6	5.23E-04	5.16E-05	6.29E-02			
Equivalent average Power Density 1.59E						

The radiated power (considering the mismatch to the 50 ohm unitary voltage source) is 1.81E-3 W, therefore a factor equal to 12188 is required to scale up to 22 W radiated. The corresponding scaled-up power densities are reported in the tables above, which show that the simulation overestimates the average power density from the MPE measurements (0.297 mW/cm²), as derived from the measured E-field reported in the following table:

Position	SE (meas), 22 W output mW/cm <sup>2</sup>
Head	0.38
Chest	0.33
Lower Trunk	0.16

The simulations tend to overestimate the average power density levels, which is understandable since there are no ohmic losses and perfect impedance matching is enforced in the computational models. Based on these results, we conclude that the simulation will produce slight exposure overestimates (about 9%).

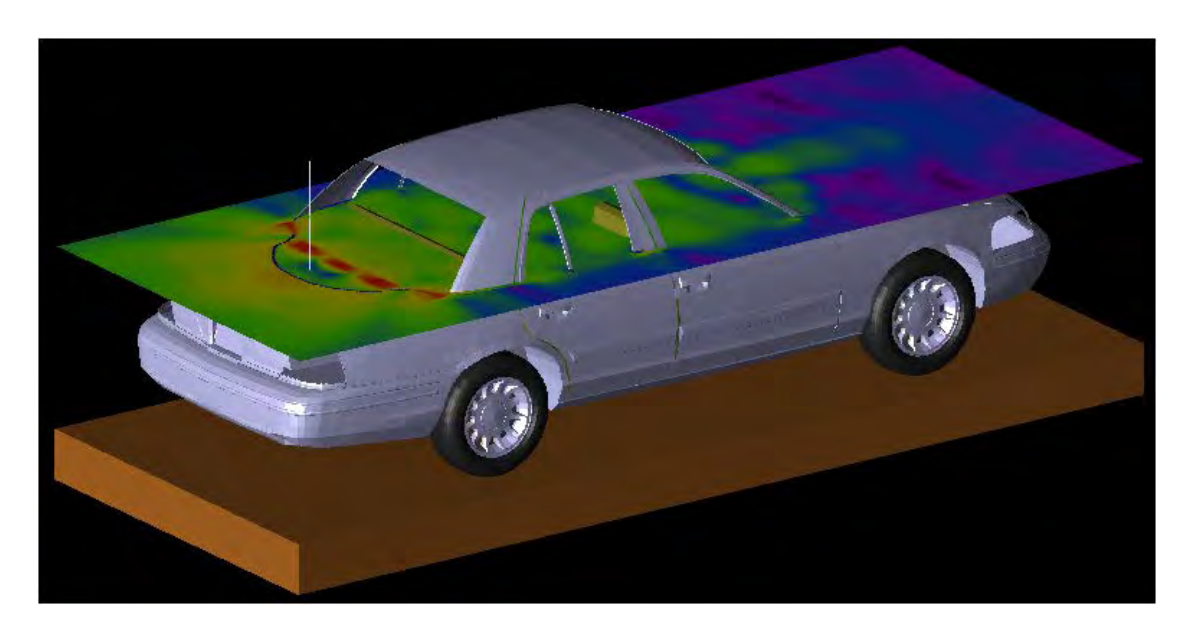
b) Descriptions and illustrations showing the correspondence between the modeled test device and the actual device, with respect to shape, size, dimensions and near-field radiating characteristics, are found in the main report.

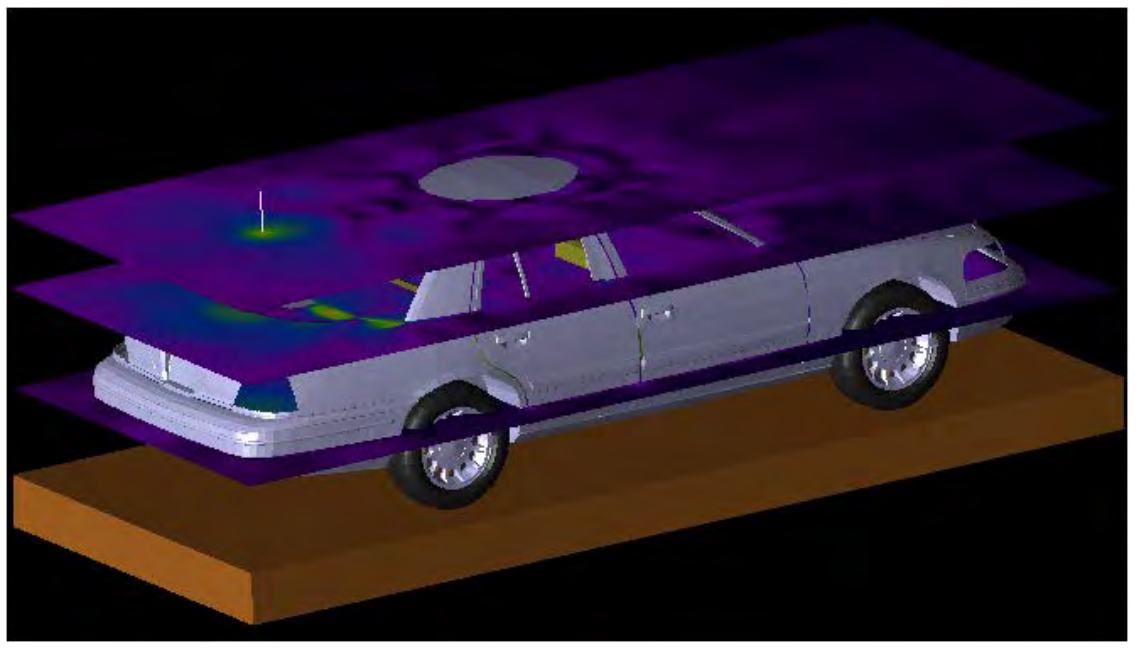
- c) Verification that the test device model is equivalent to the actual device for predicting the SAR distributions descends from the fact that the car and antenna size and location in the numerical model correspond to those used in the measurements.
- d) The peak SAR is in the neck region for the passenger, which is in line with MPE measurements and predictions.

### Passenger with 63.5 cm monopole antenna (HAE6010A 425 MHz)

The following figures show the car model with the field distribution in the horizontal planes where the MPE measurements have been performed. The comparison has been performed by taking the average of the computed steady-state field values at the three locations, corresponding to the head, chest, and lower trunk, and comparing them with the average of the MPE measurements performed at the head, chest and lower trunk locations. Such a comparison is carried out at the same average power level (61.5 W, including the 50% duty factor) used in the MPE measurements.







The equivalent power density (S) is computed from the E-field. The following table reports the E-field values computed by  $XFDTD^{TM}$  at the three locations, and the corresponding power density.

Locatio n Number	E-field, V/ m	Eq. Power Density 1.0 V source	Scaled Power Dens. 61.5 W output, mW/cm^2
1	2.26E-01	6.76E-05	0.74
2	3.60E-01	1.72E-04	1.89
3	1.40E-01	2.59E-05	0.28

Equivalent average Power Density	0.97
----------------------------------	------

The corresponding scaled-up power densities are reported in the tables above, which show that the simulation overestimates the average power density from the MPE measurements (0.52 mW/cm<sup>2</sup>), as derived from the measured E-field reported in the following table:

Position	SE (meas), 60 W output mW/cm <sup>2</sup>
Head	0.72
Chest	0.64
Lower Trunk	0.19

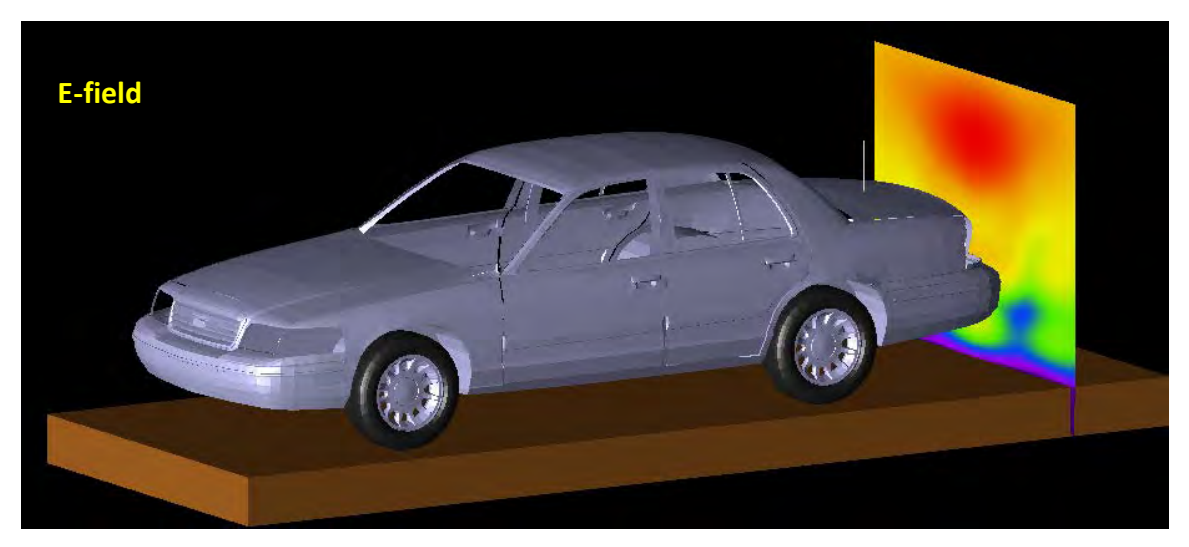
The simulations tend to overestimate the average power density levels, which is understandable since there are no ohmic losses and perfect impedance matching is enforced in the computational models. Based on these results, we conclude that the simulation will produce exposure overestimates (about 88%).

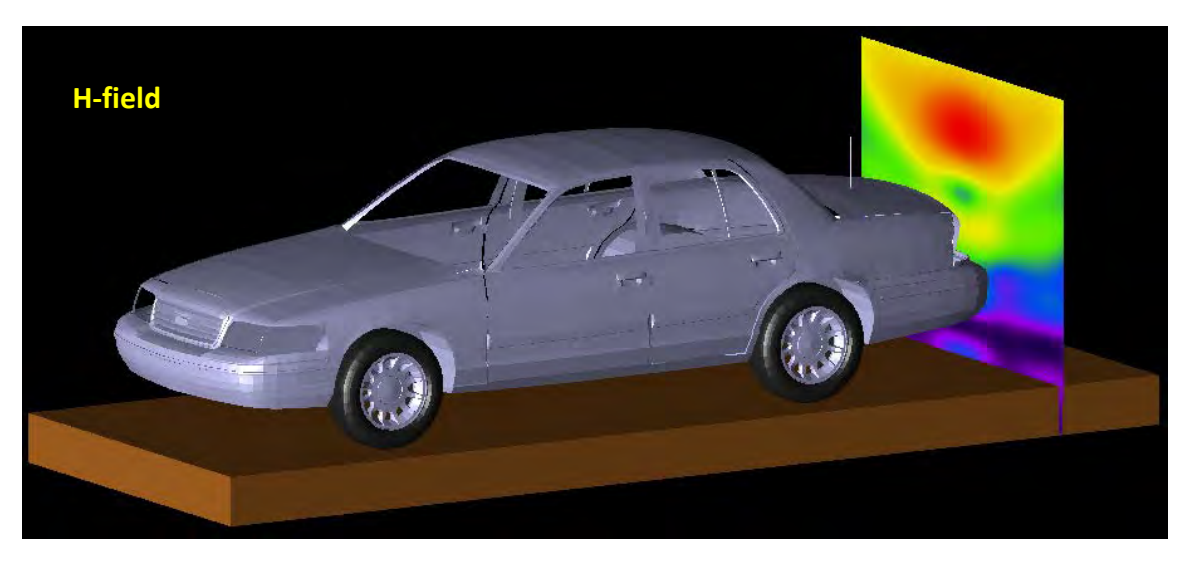
### Bystander with 29 cm monopole antenna (HAE6013A 425 MHz)

The following figures show the E-field and H-field distributions across a vertical plane passing for the antenna and cutting the car in half. As done in the measurements, the MPE is computed from both E-field and H-field distributions, along the yellow dotted line at 10 points spaced 20 cm apart from each other up to 2 m in height. These lines and the field evaluation points are approximately indicated in the figures. The E-field and H-field distributions in the vertical plane placed at 90 cm from the antenna, behind the case, are shown as well. The points where the fields are sampled to determine the equivalent power density (S) are approximately indicated by the white dots. A picture of the antenna is not reported because it is identical to the HAE6013A.





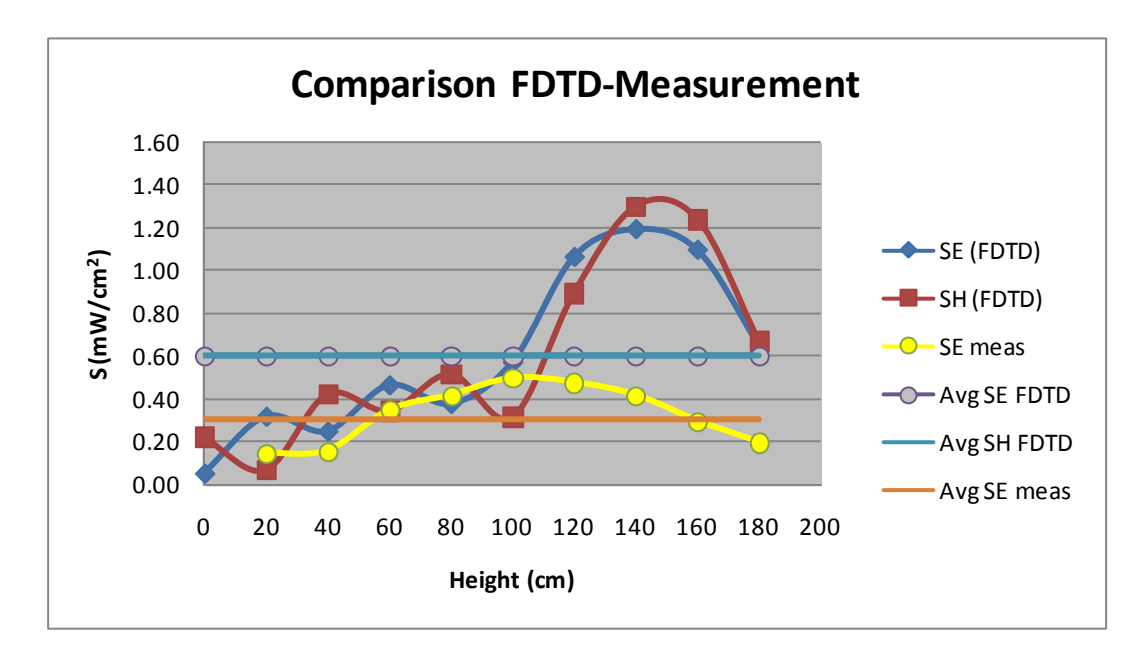




The following table reports the field values computed by  $XFDTD^{TM}$  for the 1.0 V source and the corresponding power density values. The average exposure levels are computed as well.

Height (cm)	E (V/m)	$S_{\rm E} (W/m^2)$	H (A/m)	$S_{\rm H} (W/m^2)$
0	5.67E-02	4.27E-06	3.11E-04	1.83E-05
20	1.40E-01	2.59E-05	1.78E-04	5.96E-06
40	1.24E-01	2.03E-05	4.29E-04	3.47E-05
60	1.69E-01	3.79E-05	3.88E-04	2.84E-05
80	1.52E-01	3.08E-05	4.74E-04	4.24E-05
100	1.87E-01	4.65E-05	3.71E-04	2.59E-05
120	2.56E-01	8.67E-05	6.23E-04	7.31E-05
140	2.71E-01	9.73E-05	7.50E-04	1.06E-04
160	2.60E-01	8.94E-05	7.33E-04	1.01E-04
180	2.00E-01	5.31E-05	5.40E-04	5.50E-05
Avera	age S <sub>E</sub>	4.92E-05	Average S <sub>H</sub>	4.91E-05

Since the conducted power during the MPE measurement was 123 W the calculated power density was then scaled for 61.5 W radiated power (taking into account 50% talk time). This model does not include the mismatch loss, loss in the cable and finite conductivity of the car surface and as represents a conservative model for exposure assessment. The scaled-up power density values for 61.5 W radiated power are 6.03 W/m² (E), and 6.02 W/m² (H), that correspond to 0.603 mW/cm² (E), and 0.602 mW/cm² (H). Measurements yielded average power density of 0.309 mW/cm² (E), which shows that the calculated power density is overestimated. The following graph shows a comparison between the measured power density and the simulated one, based on E or H fields, normalized to 61.5 W radiated power.



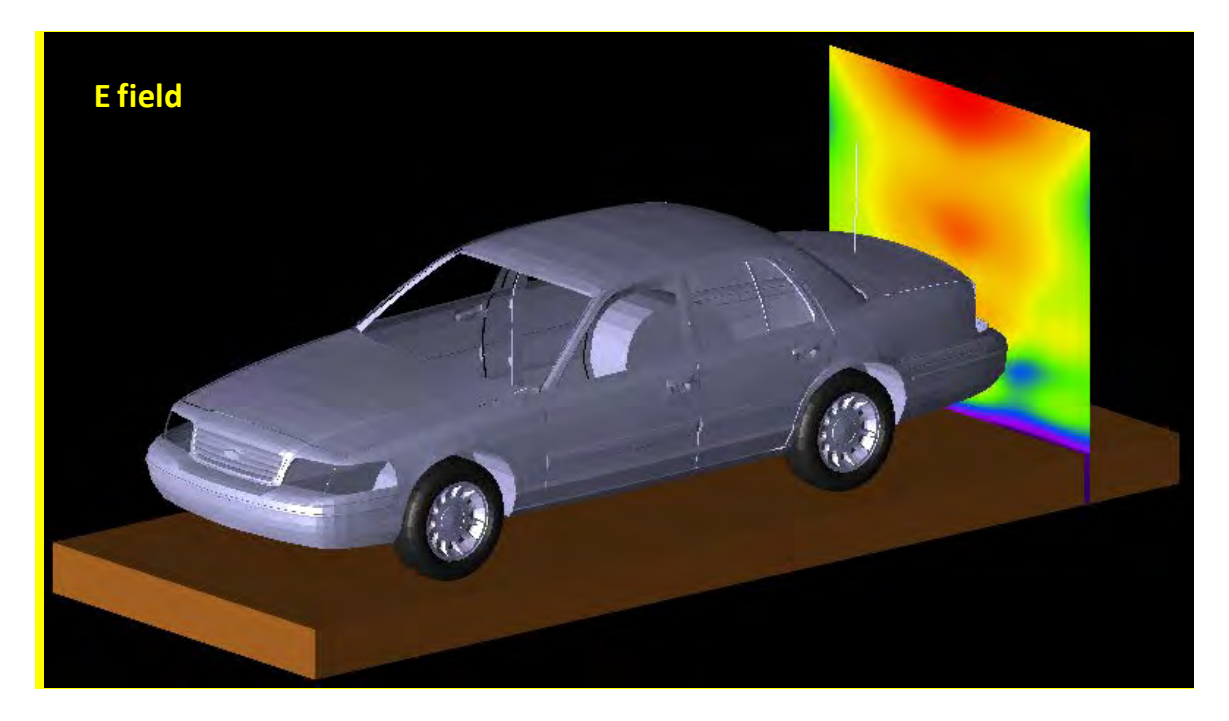
Bystander with 63.5 cm monopole antenna (HAE6010A 425 MHz)

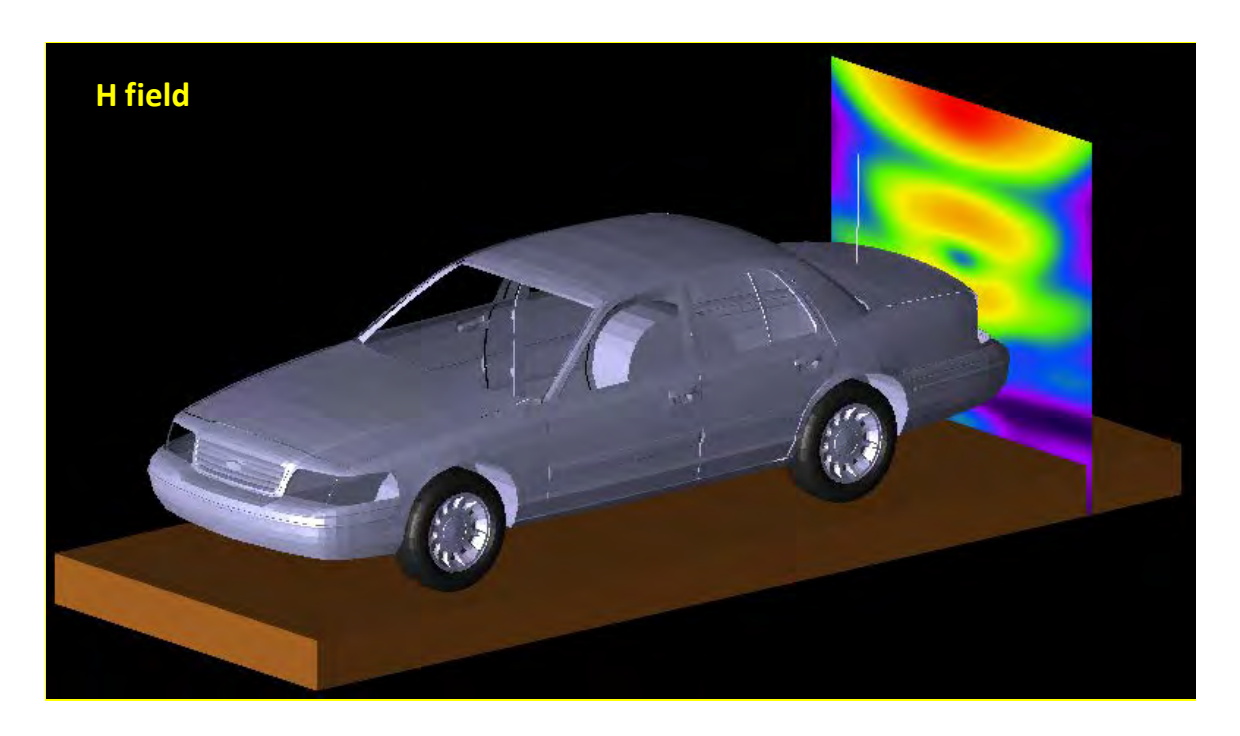
The following figures show the E-field and H-field distributions across a vertical plane passing for the antenna and cutting the car in half. As done in the measurements, the MPE is computed from both E-field and H-field distributions, along the yellow dotted line at 10 points spaced 20 cm apart from each other up to 2 m in height. These lines and the field evaluation points are

approximately indicated in the figures. The E-field and H-field distributions in the vertical plane placed at 90 cm from the antenna, behind the case, are shown as well. The points where the fields are sampled to determine the equivalent power density (S) are approximately indicated by the white dots. A picture of the antenna is not reported because it is identical to the HAE6010A.





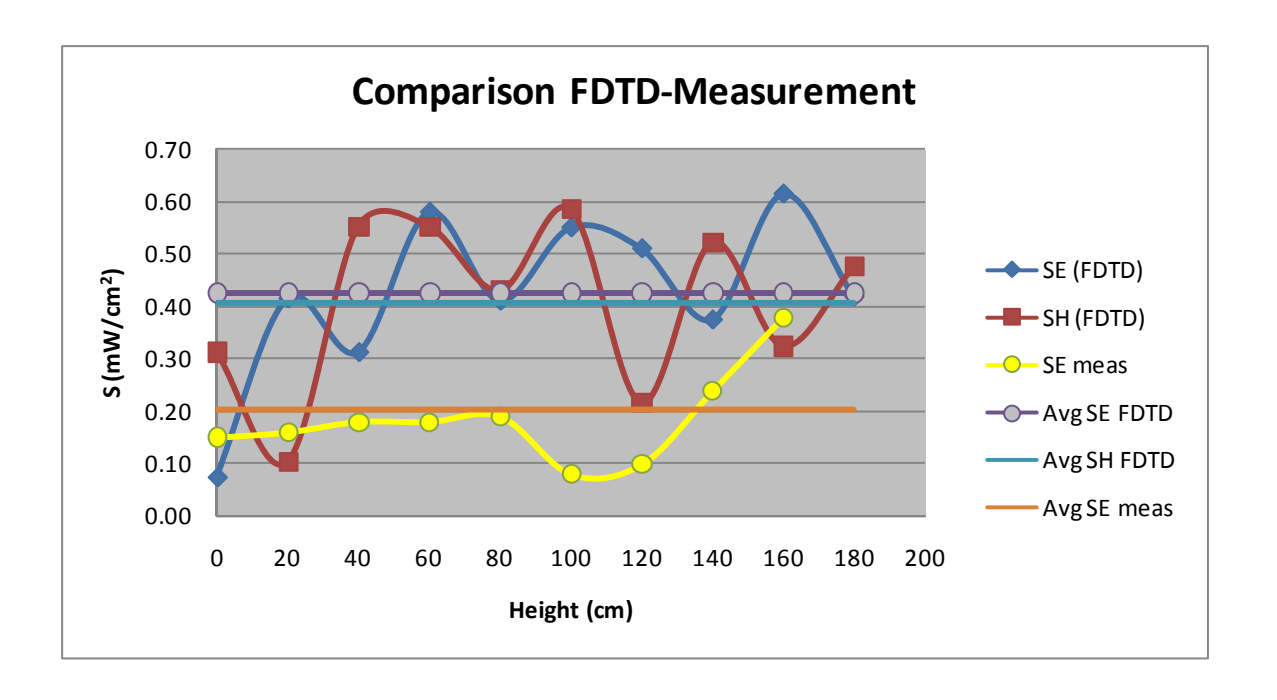




The following table reports the field values computed by XFDTD<sup>TM</sup> and the corresponding power density values. The average exposure levels are computed as well.

Height (cm)	E (V/m)	$S_{\rm E} ({ m W/m}^2)$	H (A/m)	$S_{\rm H} (W/m^2)$
0	7.55E-02	7.56E-06	4.13E-04	3.21E-05
20	1.79E-01	4.27E-05	2.37E-04	1.06E-05
40	1.56E-01	3.21E-05	5.49E-04	5.69E-05
60	2.12E-01	5.96E-05	4.84E-04	5.69E-05
80	1.78E-01	4.22E-05	5.65E-04	4.42E-05
100	2.07E-01	5.66E-05	3.43E-04	6.03E-05
120	1.99E-01	5.25E-05	5.34E-04	2.21E-05
140	1.70E-01	3.85E-05	4.20E-04	5.37E-05
160	2.18E-01	6.32E-05	5.10E-04	3.33E-05
180	1.80E-01	4.30E-05	8.15E-04	4.90E-05
Avera	age S <sub>E</sub>	4.38E-05	Average S <sub>H</sub>	4.19E-05

Since the conducted power during the MPE measurement was 123 W the calculated power density was then scaled for 61.5 W radiated power (taking into account 50% talk time). This model does not include the mismatch loss, loss in the cable and finite conductivity of the car surface and as represents a conservative model for exposure assessment. The scaled-up power density values for 61.5 W radiated power are 4.26 W/m² (E), and 4.07 W/m² (H), that correspond to 0.426 mW/cm² (E), and 0.407 mW/cm² (H). Measurements yielded average power density of 0.204 mW/cm² (E), which shows that the calculated power density is overestimated. The following graph shows a comparison between the measured power density and the simulated one, based on E or H fields, normalized to 61.5 W radiated power.



### 7) Test device positioning

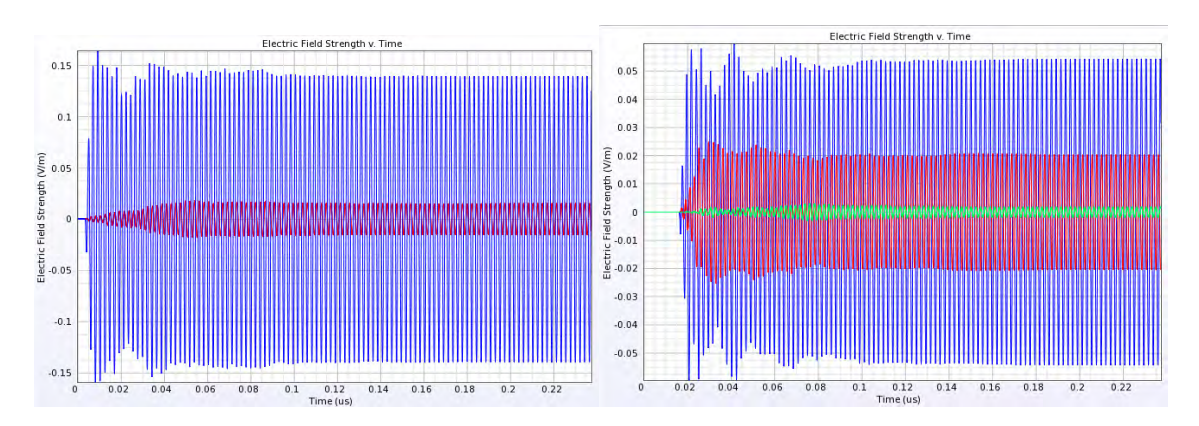
- a) A description of the device test positions used in the SAR computations is provided in the SAR report.
- b) Illustrations showing the separation distances between the test device and the phantom for the tested configurations are provided in the SAR report.

#### 8) Steady state termination procedures

FCC ID: AZ492FT7089/ ISED: 109U-92FT7089

a) The criteria used to determine that sinusoidal steady-state conditions have been reached throughout the computational domain for terminating the computations are based on the monitoring of field points to make sure they converge. The simulation projects were set to automatically track the field values throughout computational domain by means of XFDTD simulation control feature which ensures that "convergence is reached when near-zone data shows a constant amplitude sine wave – when all transients have died down and the only variation left is sinusoidal. In this case "convergence" is tested on the average electric field in the space for its deviation from a pure sine wave. XFDTD automatically places points throughout the space for this purpose." [XFDTD Reference Manual, version 7.3]. This convergence threshold was set to -60 dB.

In addition for at least one passenger and one bystander exposure condition, we placed one "field sensor" near the antenna, others between the body and the domain boundary at different locations, and one inside the head of the model. In all simulations, isotropic E-field sensors were placed at opposite sides of the computational domain. We used isotropic E and H field "sensors", meaning that all three components of the fields are monitored at these points. The following figures show an example of the time waveforms at the field point sensors in two points of the computational domain. We selected points close to antenna as well as furthest one. The highest field levels are observed for the higher index point, as it is closer to the antenna. In all cases, the field reaches the steady-state condition.



c) The XFDTD<sup>TM</sup> algorithm determines the field phasors by using the so-called "two-equations two-unknowns" method. Details of the algorithm are explained in [7].

### 9) Computing peak SAR from field components

FCC ID: AZ492FT7089/ ISED: 109U-92FT7089

a) The SAR for an individual voxel is computed according to the draft IEC/IEEE 62704-1 standard. In particular, the three components of the electric field are computed in the center of each voxel and then the SAR is computed as below:

$$SAR = \sigma_{voxel} \frac{|E_x|^2 + |E_y|^2 + |E_z|^2}{2\rho_{voxel}},$$

where  $\sigma_{varel}$  and  $\rho_{varel}$  are the conductivity and the mass density of the voxel.

### 10) One-gram and ten-gram averaged SAR procedures

- a) XFDTD™ computes the Specific Absorption Rate (SAR) in each complete cell containing lossy dielectric material and with a non-zero material density. Using the SAR values computed for each voxel of the model the averaging calculation employs the method and specifications defined in the draft IEC/IEEE 62704-1 standard to generate one-gram and ten-gram average SAR.
- 11) Total computational uncertainty We derived an estimate for the uncertainty of FDTD methods in evaluating SAR by referring to [6]. In Fig. 7 in [6] it is shown that the deviation between SAR estimates using the XFDTD<sup>TM</sup> code and those measured with a compliance system are typically within 10% when the probe is away from the phantom surface so that boundary effects are negligible. In that example, the simulated SAR always exceeds the measured SAR.

As discussed in 6(a), a conservative bias has been introduced in the model so as to reduce concerns regarding the computational uncertainty related to the car modeling, antenna modeling, and phantom modeling. The results of the comparison between measurements and simulations presented in 6(a) suggest that the present model produces an overestimate of the exposure between 4% and 36%. Such a conservative bias should eliminate the need for including uncertainty considerations in the SAR assessment.

#### 12) Test results for determining SAR compliance

- a) Illustrations showing the SAR distribution of dominant peak locations produced by the test transmitter, with respect to the phantom and test device, are provided in the SAR report.
- b) The input impedance and the total power radiated under the impedance match conditions that occur at the test frequency are provided by XFDTD<sup>TM</sup>. XFDTD<sup>TM</sup> computes the input impedance by following the method outlined in [8], which consists in performing the integration of the steady-state magnetic field around the feed point edge to compute the steady-state feed point current (I), which is then used to divide the feed-gap steady-state voltage (V). The net average radiated power is computed as

FCC ID: AZ492FT7089/ ISED: 109U-92FT7089

$$P_{XFDTD} = \frac{1}{2} \operatorname{Re} \left\{ V I^* \right\}$$

Both the input impedance and the net average radiated power are provided by XFDTD<sup>TM</sup> at the end of each individual simulation.

We normalize the SAR to such a power, thereby obtaining SAR per radiated Watt (*normalized SAR*) values for the whole body and the 1-g SAR. Finally, we multiply such normalized SAR values times the max power rating of the device under test. In this way, we obtain the exposure metrics for 100% talk-time, i.e., without applying source-based time averaging.

- c) For mobile radios, 50% source-based time averaging is applied by multiplying the SAR values determined at point 12(b) times a 0.5 factor.
- d) The final SAR values used for compliance evaluation for each simulated configuration are obtained by applying the IEC/IEEE 62704-2 draft standard adjustment factors to account for exposure variation in population.

# 13) SAR computational result adjustment to account for variations in the human body model

Peak spatial-average and whole-body average exposure varies from person to person due to physical and anatomical differences. As a result, adjustment factors to account for these variations have been determined by IEEE/IEC 62704-2 computational study [5].

To demonstrate compliance to the applicable limits, the computational results reported in Table I must be adjusted by the interpolated adjustment factors from the following tables found in draft IEEE/IEC 62704-2 (August, 2016)

# Peak spatial-average SAR adjustment factors for the passenger model and trunk mount antenna.

	Trunk mount antenna						
Frequency MHz	Back sea	at, centre	Back seat, side				
	1 g	10 g	1 g	10 g			
33	1,0	1,2	1,0	1,0			
80	1,0	1,0	1,0	1,0			
150	1,9	2,0	4,2	4,4			
450	2,4	2,4	2,0	2,3			
800	1,0	1,0	1,4	1,2			
1 000	1,3	1,1	1,0	1,0			

# Peak spatial-average SAR adjustment factors for the passenger model and roof mount antennas

FCC ID: AZ492FT7089/ ISED: 109U-92FT7089

		Centr	e roof m	ount an	tenna			Side	roof mount antenna			
Frequency MHz		seat, itre		seat, de	Fron	t seat	ı	seat, itre	Back si	seat, de	Fron	t seat
	1 g	10 g	1 g	10 g	1 g	10 g	1 g	10 g	1 g	10 g	1 g	10 g
33	1,1	1,1	1,0	1,0	1,0	1,0	1,0	1,0	1,0	1,0	1,0	1,0
80	1,0	1,0	1,3	1,4	5,8	6,5	1,0	1,0	1,0	1,0	6,3	6,1
150	1,3	1,1	1,0	1,0	1,0	1,1	1,2	1,0	1,0	1,0	1,9	1,8
450	2,6	2,3	1,7	1,4	2,3	2,6	3,9	3,8	1,8	2,3	1,0	1,0
800	2,7	2,7	1,6	1,8	1,0	1,0	2,6	2,2	1,9	1,5	2,0	1,5
1 000	2,2	2,3	1,4	1,4	1,7	2,1	5,6	4,8	2,5	3,1	1,3	1,5

# Peak spatial-average SAR adjustment factors for the bystander and trunk mounted antennas

Frequency MHz	1 g SAR factor	10 g SAR factor
30	1,0	1,0
50	1,0	1,0
75	1,0	1,1
100	1,4	1,3
150	1,3	1,3
300	1,6	1,6
450	1,5	1,8
800	1,3	2,3
1 000	1,1	2,5

# Peak spatial-average SAR adjustment factors for the bystander and roof mounted antennas

FCC ID: AZ492FT7089/ ISED: 109U-92FT7089

	Centre roof mount antenna			Side roof mount antenna				Centre and side roof		
Frequency MHz	20 cm from the vehicle		40 cm from the vehicle		20 cm from the vehicle		40 cm from the vehicle		mount antenna with bystander > 50 cm from the vehicle	
	1 g	10 g	1 g	10 g	1 g	10g	1 g	10g	1 g	10 g
33	1,3	1,2	1,3	1,0	1,4	1,3	1,2	1,0	1,0	1,0
80	1,1	1,2	1,3	1,0	1,3	1,2	1,3	1,1	1,0	1,1
150	1,4	1,3	1,2	1,0	1,2	1,3	1,3	1,4	1,3	1,3
450	1,6	1,4	1,6	1,3	1,2	1,9	1,8	2,3	1,5	1,8
800	2,5	2,3	2,6	2,4	2,0	2,0	1,4	1,4	1,5	1,8
1 000	3,2	2,8	3,4	2,9	2,2	2,2	2,8	2,5	1,5	1,8

### Whole-body average SAR adjustment factors for the passenger and trunk mount antennas

Frequency	Passenger location in the vehicle			
MHz	Back seat, centre	Back seat, side		
33	1,0	1,0		
80	1,4	1,0		
150	2,4	3,0		
450	2,8	2,6		
800	2,2	1,9		
1 000	1,9	1,7		

## Whole-body average SAR adjustment factors for the passenger and roof mount antennas

	Centr	e roof mount an	tenna	Side roof mount antenna				
Frequency	Passenger location in the vehicle							
MHz	Back seat, centre	Back seat, side	Front seat	Back seat, centre	Back seat, side	Front seat		
33	1,8	1,0	1,3	1,4	1,1	1,3		
80	1,0	1,3	8,2	1,0	1,4	8,3		
150	1,9	2,4	1,6	2,0	1,5	1,7		
450	1,8	2,9	2,5	4,7	2,7	1,8		
800	2,7	2,1	2,2	2,7	2,3	2,8		
1 000	2,8	2,4	2,3	5,7	3,1	2,7		

### Whole-body average SAR adjustment factors for the bystander and trunk mount antennas

Frequency MHz	Bystander distance from the trunk mount antenna						
	80 cm	100 cm	120 cm	> 130 cm			
30	1,0	1,0	1,0	1,0			
50	1,3	1,3	1,4	1,4			
75	1,7	2,0	2,2	2,3			
100	2,5	2,5	2,5	3,5			
150	1,9	1,9	2,5	4,5			
300	2,1	2,6	2,6	2,6			
450	1,4	1,3	1,5	2,0			
800	1,0	1,0	1,0	1,0			
1 000	1,0	1,0	1,0	1,0			

### Whole-body average SAR adjustment factors for the bystander and roof mount antennas

Frequency	Centre roof m	ount antenna	Side roof mo	ount antenna	Centre and side roof mount	
MHz	20 cm from the vehicle	40 cm from the vehicle	20 cm from the vehicle 40 cm from the vehicle		antenna with bystander > 50 cm from the vehicle	
33	1,2	1,2	1,3	1,2	1,1	
80	1,6	1,5	1,7	1,7	2,5	
150	1,6	1,5	1,8	1,8	4,5	
450	1,5	1,5	1,5	1,8	2,0	
800	1,3	1,3	1,6	1,6	1,0	
1 000	1,2	1,2	1,3	1,2	1,0	

#### **REFERENCES**

- [1] K. S. Yee, "Numerical Solution of Initial Boundary Value Problems Involving Maxwell's Equations in Isotropic Media," *IEEE Transactions on Antennas and Propagation*, vol. 14, no. 3, 302-307, March 1966.
- [2] Z. P. Liao, H. L. Wong, G. P. Yang, and Y. F. Yuan, "A transmitting boundary for transient wave analysis," Scientia Sinica, vol. 28, no. 10, pp 1063-1076, Oct. 1984.
- [3] Validation exercise: Mie sphere. Remcom Inc. (enclosed PDF)



- [4] NEC-Win PRO TM v 1.1, Nittany Scientific, Inc., Riverton, UT.
- [5] C. M. Collins and M. B. Smith, "Calculations of B1 distribution, SNR, and SAR for a surface coil against an anatomically-accurate human body model," *Magn. Reson. Med.*, 45:692-699, 2001. (enclosed TIF)



[6] Martin Siegbahn and Christer Törnevik, "Measurements and FDTD Computations of the IEEE SCC 34 Spherical Bowl and Dipole Antenna," Report to the IEEE Standards Coordinating Committee 34, Sub-Committee 2, 1998. (enclosed PDF)



[7] C. M. Furse and O. P. Gandhi, "Calculation of electric fields and currents induced in a millimeter-resolution human model at 60 Hz using the FDTD method with a novel time-to-frequency-domain conversion," Antennas and Propagation Society International Symposium, 1996. (enclosed PDF)



[8] *The Finite Difference Time Domain Method for Electromagnetics*, Chapter 14.2, by K. S. Kunz and R. J. Luebbers, CRC Press, Boca Raton, Florida, 1993.

[9] Validation of Mobile Antenna Modeling by Comparison with Near-field Measurements," Report to the IEEE Standards Coordinating Committee 34, Sub-Committee 2, 2006. (enclosed PDF)



- [10] *Antenna Theory: analysis and design*, Chapter 4, by C. A. Balanis, 2<sup>nd</sup> ed. John Wiley & Sons, Inc.
- [11] S. Gabriel, R. W. Lau, and C. Gabriel. 1996. The dielectric properties of biological tissues: III. Parametric models for the frequency spectrum of tissues. Phys. Med. Biol. 41:2271–2293.